Comparative metabonomic investigations of *Schistosoma japonicum* from SCID mice and BALB/c mice: clues to developmental abnormality of schistosome in the immunodeficient host

Rong Liu[1,2], Wen-jun Cheng[1], Hong-bin Tang[3], Qin-ping Zhong[1], Zhen-ping Ming[1], Hui-fen Dong[1,2#]

1 School of Basic Medical Sciences, Wuhan University, Wuhan 430071, P. R. of China

2 Hubei Province Key Laboratory of Allergy and Immunology, School of Basic Medical Sciences, Wuhan University, Wuhan 430071, P. R. of China

3 Laboratory Animal Center, School of Medicine, Wuhan University, Wuhan 430071, P. R. of China

 # Correspondence should be addressed to: School of Basic Medical Sciences, Wuhan University. 185 Donghu Road, Wuhan 430071, P. R. of China. Fax: +86 (027) 68759222; E-mail: hfdong@whu.edu.cn (Dong H-F).

Abstract

It has been discovered that the development of schistosome is hampered in immunodeficient mice, e.g. nude mice lacking T-lymphocytes and the severe combined immune deficient (SCID) mice lacking both T- and B-lymphocytes. However, it's still unresolved about the underlying regulatory mechanisms of the retarded growth and development of schistosomes in their immunodeficient definitive host. In this study, therefore, five replicates of male or female *Schistosoma japonicum* samples with twenty male or female worms in each sample, were collected from SCID mice or BALB/c mice at five weeks post infection and used to perform metabonomic analysis using liquid chromatography tandem mass spectrometry (LC-MS/MS) platform, for elucidating the growth and development regulation of schistosome in their definitive hosts from the metabolomic aspect. Based on the identified 1015 ion features in ESI+ mode and 342 ion features in ESI- mode, multivariate modelling methods including the Principal Component Analysis (PCA), Partial Least Squares Discriminant Analysis (PLS-DA) and Orthogonal Partial Least Squares Discriminant Analysis (OPLS-DA) identified distinct metabolic profiles that clearly differentiated both male and female worms in SCID mice from those in BALB/c mice, respectively. Common and uniquely perturbed metabolites and their involved metabolic pathways were identified in male and female worms from SCID mice when compared with those from BALB/c mice. The results also revealed that more differential metabolites were found in female worms (one metabolite was up-regulated and forty metabolites were down-regulated) than male worms (nine metabolites were up-regulated and twenty metabolites were down-regulated) between SCID mice and BALB/c mice. The top five increased metabolites of male worms in SCID mice when compared with those in BALB/c mice were PC(22:6/20:1), L-allothreonine, L-serine, glycerophosphocholine and 5-

aminoimidazole ribonucleotide. And the top five decreased metabolites of male worms in SCID mice when compared with those in BALB/c mice were PC(16:0/0:0), PAF C-16, PE(18:1/0:0), adenosine and butenoyl PAF. Most of the differential metabolites of female worms in SCID mice had lower levels when compared with the normal female worms in BALB/c mice, except for retinyl ester with a higher level. The top five decreased metabolites of female worms in SCID mice when compared with those in BALB/c mice were adrenic acid, 5-phosphoribosylamine, PC(16:0/0:0), PC(22:6/20:1) and ergothioneine. The involved metabolic pathways of the differential metabolites in male worms between SCID mice and BALB/c mice mainly included taurine and hypotaurine metabolism, glycerophospholipid metabolism, sphingolipid metabolism, arachidonic acid metabolism, alpha-linolenic acid metabolism, etc. The involved metabolic pathways of differential metabolites in female worms included mainly pyrimidine metabolism, sphingolipid metabolism, arachidonic acid metabolism, glycerophospholipid metabolism, tryptophan metabolism, etc. These findings suggested a correlation between the retarded growth and development of schistosome in SCID mice and their perturbed metabolic profiles, which also provided a new insight into the regulation mechanisms of growth and development of *S. japonicum* worms from the metabolic level, and provided clues for discovery of drugs or vaccines against the parasites and parasitic disease.

Keywords: *Schistosoma japonicum*; SCID mouse; BALB/c mouse; growth and development; metabolomics; LC-MS/MS

Author summary

The growth and development of schistosome has been discovered hampered in the immunodeficient hosts. But it remains unresolved about the molecular mechanisms involved in this. In this study, we tested and compared the metabolic profiles of the male and female *Schistosoma japonicum* worms collected from SCID mice or BALB/c mice at five weeks post infection using liquid chromatography tandem mass spectrometry (LC-MS/MS) platform. There were 1015 ion features in ESI+ mode and 342 ion features in ESI- mode were identified, and distinct metabolic profiles were found to clearly differentiate both male and female worms in SCID mice from those in BALB/c mice, respectively. The results also found more differential metabolites in female worms than in male worms between SCID mice and BALB/c mice. The enriched metabolic pathways of the differential metabolites in male worms between SCID mice and BALB/c mice included taurine and hypotaurine metabolism, glycerophospholipid metabolism, sphingolipid metabolism, arachidonic acid metabolism, alpha-linolenic acid metabolism, etc. And the enriched metabolic pathways of differential metabolites in female worms included pyrimidine metabolism, sphingolipid metabolism, arachidonic acid metabolism, glycerophospholipid metabolism, tryptophan metabolism, etc. The findings in this study suggested an association between the developmentally stunted schistosome and their perturbed metabolites and metabolic pathways, which provided a new insight into the regulation mechanisms of growth and development of *S. japonicum* worms from the metabolic level, and clues for discovery of drugs or vaccines against the parasites and disease.

Introduction

Schistosomiasis, caused by infection with a parasitic blood fluke of the genus *Schistosoma*, of which *Schistosoma mansoni*, *S. haematobium* and *S. japonicum* are of particular health significance, is still one of the most serious neglected tropical disease in the endemic countries [1, 2]. Unlike other trematodes, adult schistosomes are dioecious and display a fascinating codependency in that the female worm is dependent on the male to grow and sexually mature, by residing in the male's gynecophoral canal [3]. The adult worms in pairs inhabit the mesenteric veins in the portal venous system of host, and every sexually mature female worm release thousands of eggs each day. And eggs deposited in the liver, intestinal wall and other tissues are unfortunately the main pathogenic factor to the severe schistosomiasis [3]. The highly evolved host-parasite relationship, especially that between schistosomes and their definitive hosts, is complex and long-lived [4-9].

Interestingly, however, it was found that schistosomes showed retarded growth, development and reproduction in the immunodeficient mammalian hosts, resulting in attenuated pathogenesis with decreased egg-laying and hepatic granulomas formation in the hosts [10-15]. Some researches focusing mainly on the host revealed that the host's factors interleukin (IL)-2 and IL-7 indirectly modulated the development of blood fluke through CD4+ T cells lymphocytes [10, 11, 14]. TNF was also identified to participate in maintaining the viability of adult worms with independence of the receptors TNFR1 and TNFR2 [6]. However, few researches is available about the schistosomes' molecular regulation on their growth and development.

Metabolic profile investigation is a promising approach to identify the key molecules or signaling pathways competent for addressing the phenotypic differences between worms from

different hosts [16-29]. Ultra high performance liquid chromatography and mass spectroscopy (HPLC-MS) is capable of simultaneously detecting a wide range of small molecule metabolites and providing a "metabolic fingerprint" of biological samples, and has been used as a well-established analytical tool with successful application in different fields, e.g., studying of disease progress, detection of metabolites of inborn defects, phenotypic differentiation of experimental animal models [30-32]. In this study, therefore, we tested and compared the metabonomic perturbations of *S. japonicum* worms with sex separation from the severe combined immunodeficient (SCID) mice at the fifth week post-infection, which were compared with those from BALB/c mice as the normal control. The results will provide new insights into understanding of the molecular regulations of growth and development of schistosomes in their hosts from the metabolic level, as well as clues for discovery of drugs and vaccines against the parasites and disease.

Materials and Methods

Ethics statement

All experiments using the *S. japonicum* parasite, *Oncomelania hupensis* (*O. hupensis*) snails, and mice were performed under protocols approved by Wuhan University Center for Animal Experiments (WUCAE) according to the Regulations for the Administration of Affairs Concerning Experimental Animals of China (Ethical approval number: 2016025).

Parasites and animals

O. hupensis snails infected with *S. japonicum* were purchased from the Institute of Parasitic Disease Control and Prevention, Hunan Province, China. Immunocompetent BALB/c mice and

severe combined immunodeficient (SCID) mice of BALB/c genetic background, approximately 6~8 weeks old, were purchased from Beijing Hua Fu Kang Bioscience Co. Inc (http://www.hfkbio.com/) via WUCAE. Cercariae were released by exposing the infected snails in aged tap water under a light for a minimum of 2 hours at 25ºC, and were used to infected the above two kinds of mice via percutaneous exposure at approximately 40±1 cercariae per mouse after twelve days of acclimatization. Adult worms were collected by hepato-portal perfusion of mice with phosphate buffered solution (PBS) on the 35th day post infection according to our previous research [12]. The worms were washed with PBS twice and separated manually using dissecting needle carefully under an anatomical lens if necessary, and were finally allocated 20 worms for each aliquot labeled as (1) IB-MALE, (2) IB-FEMALE, (3) IS-MALE or (4) IS-FEMALE, respectively. All the samples were frozen immediately in liquid nitrogen and then stored at -80 ºC until use for metabolite extraction. In addition, the blood of mice was collected and serum was isolated and stored at -80 ºC for serum metabolomics investigation, the paper about which was submitted elsewhere.

Sample preparation

Totally 20 frozen schistosome samples in the above four groups with five replicate samples in each group were sent to Wuhan Anlong Kexun Co., LTD (www.anachro.com.cn) for metabonomic detection and analysis using HPLC-MS/MS. The LC-MS grade methanol and acetonitrile was purchased from Merck & Co., Inc., and formic acid was from Sigma-Aldrich Co. LLC. Other reagents were all analytically pure. The schistosome samples were thawed and ground after adding 0.5 ml of methanol/distilled water (8:2, v/v) with 4 μg/ml of 2-Chloro-L-phenylalanine as the internal standard substance, and were then centrifuged at 13000 rpm

under 4 ºC for 10 min. 200 µl of supernatant from each sample was carefully transferred to a vial of autosampler for examination. All samples were kept at 4°C and analyzed in a random manner. Additionally, isometric supernatant from each sample of the above four groups were mixed for QC sample. The QC sample was run after every 2 tested samples to monitor the stability of the system.

Metabolomics analysis by HPLC-MS/MS

Liquid chromatography was performed on a 1290 Infinity UHPLC system (Agilent Technologies, Santa Clara, CA, U.S.A.). The separation of all samples was performed on an ACQUITY UPLC @HSS T3 column (Waters, U.K.) (100 mm * 2.1 mm, 2.5 µm). A gradient elution program was run for chromatographic separation with mobile phase A (0.1% formic acid in water) and mobile phase B (0.1% formic acid in acetonitrile) as follows: 0~2 min, 95%A-95%A; 2~13 min, 95%A-5%A; 13~15 min, 5%A-5%A. The sample injection volume was 3 µL and the flow rate was set as 0.4 mL/min. The column temperature was set at 25°C, and the post time was set as 5 min.

A 6538 UHD and Accurate-Mass Q-TOF (Agilent Technologies, Santa Clara, CA, USA) equipped with an electrospray ionization (ESI) source was used for mass spectrometric detection. The electrospray ionization mass spectra for sample analysis were acquired in both positive ion mode (ESI+) and negative ion mode (ESI-). The operating parameters were as follows: capillary, 4000 V (ESI+) or 3000 V (ESI-); sampling cone: 45 V; source temperature: 110 °C (ESI+) or 120 °C (ESI−); desolvation temperature: 350 °C; desolvation gas, 11 L/min; source offset (skimmer1): 60 V; TOF acquisition mode: sensitivity (ESI+) or sensitivity (ESI−); acquisition method, continuum MSE; TOF mass range: 100-1000 Da; scan time: 0.2 s;

collision energy function 2: trap CE ramp 20 to 40 eV. Quality control (QC) samples were used in order to assess the reproducibility and reliability of the LC-MS/MS system. QC samples prepared as mentioned above were used to provide a 'mean' profile representing all analyses encountered during the analysis. The pooled 'QC' samples were run before and after every two study samples to ensure system equilibration. Two reference standard compounds purine ($C_5H_4N_4$) (with m/z 121.0509 in ESI+ mode and m/z 119.0363 in ESI- mode) and hexakis (1H,1H,3H-tetrafluoro-pentoxy)-phosphazene ($C_{18}H_{18}O_6N_3P_3F_{24}$) (with m/z 922.0098 in ESI+ mode and m/z 966.0007 in ESI- mode) were continuously infused into the system to allow constant mass correction during the run.

Metabolic data analysis

Raw spectrometric data were uploaded to and analyzed with the MassHunter Qualitative Analysis B.04.00 software (Agilent Technologies, USA) for untargeted peak detection, peak alignment, peak grouping, normalization and integration on each full data set (study samples and QC samples). The molecular features, characterized by retention time (RT), chromatographic peak intensity, and accurate mass, were obtained by using the Molecular Feature Extractor algorithm. The features were then analyzed with the MassHunter Mass Profiler Professional software (Agilent Technologies). Only features with an intensity of ≥ 20,000 counts (approximately three times the detection limit of the LC-MS/MS instrument used in this study) that were found in at least 80% of the samples at the same sampling time point were kept for further processing. Next, a tolerance window of 0.15 min and 2 mDa was used for alignment of retention time and m/z values, and the data were also normalized by the internal standard 2-Chloro-L-phenylalanine added when sample preparation. The data matrix

was then mean-centered and Pareto-scaled prior to multivariate analysis (MVA) using Principal Component Analysis (PCA), Partial Least Squares Discriminant Analysis (PLS-DA) and Orthogonal Partial Least Squares Discriminant Analysis (OPLS-DA) to discriminate comparison groups using the function module *Statistical Analysis* on the online application *MetaboAnalyst* (http://www.metaboanalyst.ca/) [33-35]. The quality of the models was evaluated with the relevant parameters R^2 and Q^2, which were discussed elsewhere (Lee et al., 2003). And differences between groups (IS-MALE *vs.* IB-MALE, and IS-FEMALE *vs.* IB-FEMALE) were determined using Student's *t*-test, and the adjusted *P* value (false discovery rate, FDR) of <0.05 was considered to be of statistical significance. Fold change (FC) analysis, which was used to show how the selected differential metabolites varied between the compared groups, was also performed to further filter the features/metabolites of particular concern with an FC of ≥1.2 or ≤0.8 between the compared groups.

The structure identification of the differential metabolites was based on the methods described as follows. Briefly, the element compositions of the metabolites were first calculated with MassHunter software from Agilent based on the exact mass, the nitrogen rule, and the isotope pattern. Then, the elemental composition and exact mass were used for open source database searching, including LIPIDMAPS (http://www.lipidmaps.org/), HMDB (http://www.hmdb.ca/), METLIN (http://metlin.scripps.edu/), and MassBank (http://www.massbank.jp/). Next, MS/MS experiments were performed to obtain structural information via the interpretation of the fragmentation pattern of the metabolite. The MS/MS spectra of possible metabolite candidates in the databases were also searched and matched.

MetaboAnalyst was used to perform metabolic pathway analysis of the differentially expressed metabolites. The identified pathways associated with the abnormal growth and

development of schistosome in SCID mice are presented according to the *P*-values from the pathway enrichment analysis (y-axis) and pathway impact values from pathway topology analysis (x-axis), with the most impacted pathways colored in red color.

Results

Metabolic profiles

All total ion chromatograms (TIC) of QC samples exhibited stable retention times without obvious peaks' drifts (Figure S1), which indicated good capability of the LC-MS/MS based-metabolomics approach used in this study. Totally, 1015 ion features in ESI+ mode and 342 ion features in ESI- mode were obtained in all the male or female *S. japonicum* worms samples, respectively. The stability and reproducibility of the HPLC-MS/MS method was evaluated by performing principal components analysis (PCA) on all the samples, together with 10 QC samples. The QC samples are generally clustered closely to each other and are separated from the tested samples in the two-dimensional PCA score plots (Figure 1-A, B) and PLS-DA score plots (Figure 1-C, D), though a moderate separation among the QC samples in ESI+ mode was observed (Figure 1-A), which confirms good stability and reproducibility of the chromatographic separation during the whole sequence. In addition, although the male worms (both IS-MALE and IB-MALE) were clearly separated from the female worms (both IS-FEMALE and IB-FEMALE), the male worms IS-MALE and IB-MALE were partially overlapped in the two-dimensional PCA score plots in both ion modes (Figure 1-A, B), while the female worms IS-FEMALE and IB-FEMALE were completely separated in ESI- mode (Figure 1-B), which indicated larger differences between male and female worms than the differences between the worms of the same sex derived from two different hosts, and

larger differences between IS-FEMALE and IB-FEMALE than that between IS-MALE and IB-MALE. Similar results were also found in the two-dimensional PLS-DA models performed on all the samples, and it yielded distinct separation of the tested four groups of worms in both ESI+ (Figure 1-C) and ESI- mode (Figure 1-D).

Metabolomic profiles distinguish between *S. japonicum* worms from SCID mice and those from BALB/c mice

Score scatter plots for two-dimensional OPLS-DA model in both ESI+ mode (Figure 2-A) and ESI- mode (Figure 2-B) showed good discrimination between the male worms from SCID mice and those from BALB/c mice (IS-MALE *vs*. IB-MALE), which was also demonstrated in the heatmap based on the differential metabolites of the 10 male worms samples (Figure 2-C). Likewise, the score plots for two dimensional OPLS-DA mode in both ESI+ mode (Figure 2-D) and ESI- mode (Figure 2-E) also showed distinct group separation between the female worms samples from SCID mice and those from BALB/c mice (IS-FEMALE *vs*. IB-FEMALE), which was further supported by the heatmap constructed based on the 10 female worms samples (Figure 2-F).

Patterns of metabolites with differential amount in schistosome

Twenty-nine differential ion features/metabolites (FDR<0.05, and FC ≥1.2 or ≤0.8), with nine increased and twenty decreased, were identified between IS-MALE *vs*. IB-MALE (Table S1, Figure 2-C). Five of the increased metabolites, PC(22:6/20:1) (which was traditionally named as lecithin), L-allothreonine, L-serine, glycerophosphocholine, and 5-aminoimidazole ribonucleotide, even had an FC >1.5, particularly for PC(22:6/20:1) involved in the

glycerophospholipid metabolism having an FC of 17.53 between IS-MALE *vs*. IB-MALE. None of the twenty decreased metabolites had an FC <0.5 between IS-MALE *vs*. IB-MALE. Meanwhile, forty-one differential features/metabolites were identified between IS-FEMALE and IB-FEMALE (Table S2, Figure 2-F). Retinyl ester, a metabolite of the retinol metabolism pathway, is the only metabolite that showed up-regulated between IS-FEMALE and IB-FEMALE. Four of the remained forty decreased metabolites, 5-phosphoribosylamine, PC(16:0/0:0), PC(22:6/20:1) and ergothioneine, even had an FC <0.5 between IS-FEMALE and IB-FEMALE.

Comparison of differential metabolic profiles between IS-MALE *vs*. IB-MALE and IS-FEMALE *vs*. IB-FEMALE found that eleven features/metabolites were common in their differential metabolites (Table 1, Figure 3-A, B). Most of the common differential metabolites in both male and female worms had the similar decrease trend in the SCID mice, except that PC(22:6/20:1) increased in male worms but decreased in female worms in SCID mice compared with BALB/c mice (Table 1 and Figure 3-B). After removing the common differential metabolites, eighteen differential metabolites were distinct in IS-MALE *vs*. IB-MALE (Table 2, Figure 3-C), and thirty differential metabolites were distinct in IS-FEMALE *vs*. IB-FEMALE (Table 3, Figure 3-D), which is more than male worms. These differential metabolites common and distinct in male worms or female worms in SCID mice compared with BALB/c mic may be associated with the abnormal growth and development of worms in SCID mice, and the differential metabolites distinct in male worms or female worms should be associated with larger differences between IS-FEMALE and IB-FEMALE than those between IS-MALE and IB-MALE.

Table 1 List of the common differential metabolites in male and female worms from SCID mice

ESI Mode	m/z	RT (min)	Male worms			Female worms			Metabolites
			P value	FDR	FC(M_{IS}/M_{IB})	*P* value	FDR	FC(F_{IS}/F_{IB})	
+	550.387	12.1807	3.21E-05	0.000546	0.54	0.000218	0.001573	0.57	Butenoyl PAF
+	152.0568	1.4347	0.022438	0.027246	0.79	0.003534	0.006597	0.74	Guanine
+	205.0975	3.9998	0.009361	0.013994	0.75	0.00142	0.003787	0.61	L-Tryptophan
+	548.3715	11.2785	0.000244	0.001152	0.65	0.001202	0.003416	0.64	LysoPC(20:2)/ PC(O-18:2/2:0)/ PC(20:2/0:0)
+	578.4181	13.7448	7.20E-05	0.000612	0.66	4.00E-05	0.000746	0.57	LysoPC(22:1)/ PC(22:1/0:0)
+	524.3717	11.9213	0.000386	0.001458	0.62	0.000301	0.001573	0.63	PAF C-16
+	552.4029	13.4095	0.001334	0.004072	0.67	0.012797	0.01586	0.72	PAF C-18
+	496.3402	10.5067	0.000265	0.001152	0.62	0.024157	0.027552	0.47	PC(16:0/0:0)
+	860.6126	14.5507	0.00236	0.005349	17.53	0.009766	0.012718	0.31	PC(22:6/20:1)
+	454.2931	10.5736	0.000823	0.002798	0.72	0.00111	0.003416	0.60	PE(16:0/0:0)
+	460.2796	10.9475	1.99E-05	0.000546	0.63	0.000269	0.001573	0.65	PE(P-16:0/0:0)

ESI mode: +, positive ion mode; -, negative ion mode. m/z: mass-to-charge ratio. RT: retention time. FDR: false discovery rate. FC: fold change.

Table 2 List of the male worm-specific differential metabolites between SCID mice and BALB/c mice

ESI Mode	m/z	RT(min)	*P* values	FDR	FC (M_{IS}/M_{IB})	Metabolites
-	118.0509	0.6543	0.017517	0.023823	1.88	L-Allothreonine
-	104.0354	0.6497	0.008371	0.013552	1.81	L-Serine
+	258.1101	0.6723	0.004564	0.008621	1.78	Glycerophosphocholine
+	296.0658	0.6469	0.00484	0.008661	1.57	5-Aminoimidazole ribonucleotide
-	179.0556	0.654	0.049459	0.049459	1.27	L-(+)-Gulose
-	102.0549	0.6795	0.01748	0.023823	1.26	N-Ethylglycine
-	124.0058	0.6871	0.003978	0.007956	1.26	Taurine
-	199.0373	0.6377	0.041292	0.043873	1.21	L-Fucose
+	146.1176	3.6118	0.04623	0.047631	0.79	Acetylcholine
+	282.2795	9.3158	0.003731	0.007928	0.78	Oleamide
+	300.2902	9.3158	0.000153	0.001038	0.78	Sphingosine
+	482.3605	10.8804	0.009467	0.013994	0.73	Lyso-PAF C-16
+	508.3405	12.2338	0.001437	0.004072	0.73	Gymnodimine
+	576.4024	12.5121	0.000271	0.001152	0.72	LysoPC(22:2)
+	520.3399	10.1254	0.001677	0.004386	0.72	PC(18:2/0:0)
+	302.3053	9.016	0.000153	0.001038	0.67	Sphinganine
+	480.309	10.8995	4.90E-05	0.000556	0.61	PE(18:1/0:0)
+	268.1045	1.2762	0.005214	0.008864	0.57	Adenosine

ESI mode: +, positive ion mode; -, negative ion mode. m/z: mass-to-charge ratio. RT: retention time.

FDR: false discovery rate. FC: fold change.

Table 3 List of the female worm-specific differential metabolites between SCID mice and BALB/c mice

ESI Mode	m/z	RT(min)	*P* values	FDR	FC (F_{IS}/F_{IB})	Metabolites
-	301.2171	12.9477	0.000132	0.001233	2.34	Retinyl ester
+	269.0885	1.4201	0.003199	0.006398	0.80	Arabinosylhypoxanthine
-	464.3143	12.3082	0.025349	0.027741	0.80	PC(P-15:0/0:0)/PE(P-18:0/0:0)/PE(O-18:1/0:0)
+	137.046	1.4199	0.000225	0.001573	0.79	Hypoxanthine
-	191.0178	0.8004	0.008998	0.011998	0.79	Citric acid/Isocitric acid/Diketogulonic acid/ 2,3-Diketo-L-gulonate
-	596.3926	13.4124	0.010324	0.013139	0.79	CerP(18:1/12:0)
+	284.0993	1.4349	0.025797	0.027741	0.78	Guanosine
+	298.0974	4.0607	0.00461	0.007822	0.78	5'-Methylthioadenosine
+	123.0554	1.0077	0.001965	0.004584	0.77	Niacinamide
-	267.0717	1.4171	0.002114	0.004735	0.76	Inosine
-	256.0576	0.6944	0.007146	0.010815	0.76	N-Acetylmannosamine/N-Acetyl-b-D-galactosamine/Beta-N-Acetylglucosamine/N-Acetylgalactosamine
-	219.0968	0.6785	0.0246	0.027552	0.72	N-Acetyl-b-glucosaminylamine
-	327.2327	13.3711	0.00792	0.011671	0.71	Docosahexaenoic acid
-	592.3605	11.2786	0.004009	0.007241	0.69	PC(16:0/5:0(CHO))

+	132.1019	1.172	0.004177	0.00731	0.68	L-Isoleucine
-	480.309	11.876	0.00122	0.003416	0.67	LysoPC(15:0)/LysoPE(0:0/18:0)/PC(14:0/O-1:0)/PC(7:0/O-8:0)/PE(18:0/0:0)/PC(15:0/0:0)
-	293.1175	4.4634	0.003346	0.006462	0.67	Glutamylphenylalanine
-	557.3195	10.6175	0.000432	0.001862	0.66	Oleic Acid-biotin
+	182.0811	1.1304	0.001879	0.004574	0.65	L-Tyrosine
-	146.0449	0.6795	0.013028	0.01586	0.64	L-Glutamic acid
-	540.3297	10.6169	0.000736	0.002944	0.64	(25R)-3alpha,7alpha-dihydroxy-5beta-cholestan-27-oyl taurine / LysoPC(P-18:1)/C-8 Ceramide-1-phosphate
-	452.2769	10.5719	0.002999	0.006219	0.63	LysoPE(0:0/16:0)/PE(16:0/0:0)/PC(13:0/0:0)
-	281.2481	14.5325	7.09E-05	0.000794	0.63	Vaccenic acid/Oleic acid
-	535.1528	1.4173	0.001719	0.004375	0.59	1,4-beta-D-Glucan/Isocaviunin 7-O-glucoside
+	146.0602	4.0002	0.000858	0.003004	0.58	4-formyl Indole
-	303.2326	13.5603	0.000836	0.003004	0.56	Arachidonic acid
-	478.2923	10.9031	0.000403	0.001862	0.55	LysoPE(0:0/18:1)
-	331.2635	14.2904	0.000309	0.001573	0.51	Adrenic acid
-	264.005	0.7038	2.66E-05	0.000745	0.50	5-Phosphoribosylamine
+	230.0967	0.7226	7.35E-07	4.12E-05	0.29	Ergothioneine

1 ESI mode: +, positive ion mode; -, negative ion mode. m/z: mass-to-charge ratio. RT: retention time.

2 FDR: false discovery rate. FC: fold change.

3

By searching against "The Human Metabolome Database" (HMDB, access via http://www.hmdb.ca/) for metabolite classification, "glycerophospholipids", "organonitrogen compounds" and "carboxylic acids and derivatives" were found as the top three categories (≥ 3 differential metabolites involved) of differential metabolites between IS-MALE *vs*. IB-MALE (Figure 4-A). Metabolite set enrichment analysis (MSEA, access via http://www.metaboanalyst.ca/) found that "bile acid biosynthesis", "taurine and hypotaurine metabolism", "sphingolipid metabolism", "retinol metabolism", "purine metabolism", "fructose and mannose degradation", "ammonia recycling", "glycine and serine metabolism", "homocysteine degradation", "phosphatidylethanolamine biosynthesis", "methionine metabolism" and "selenoamino acid metabolism" were the prominently enriched metabolite sets (with adjusted *P* values < 0.05) based on the differential metabolites between IS-MALE *vs*. IB-MALE (Table S3, Figure 4-B). Meanwhile, "glycerophospholipids", "carboxylic acids and derivatives", "organonitrogen compounds", "fatty acyls" and "purine nucleosides" were the top five enriched categories of differential metabolites between IS-FEMALE *vs*. IB-FEMALE (Figure 4-C). And MSEA based on the differential metabolites between IS-FEMALE *vs*. IB-FEMALE found that "retinol metabolism", "alpha linolenic acid and linoleic acid metabolism", "purine metabolism", "sphingolipid metabolism" and "glutamate metabolism" were the prominently enriched metabolite sets with raw P values < 0.05 but only "retinol metabolism" has an adjusted *P* value < 0.05 (Table S4, Figure 4-D). Moreover, most (9/11) of the common differential metabolites between IS-MALE *vs*. IB-MALE and IS-FEMALE *vs*. IB-FEMALE belong to glycerophospholipids (Figure 4-E), which was enriched by MSEA to phospholipid biosynthesis (Table S5, Figure 4-F). The differential metabolites distinct in IS-MALE *vs*. IB-MALE were classified prominently into "organonitrogen compounds", "glycerophospholipids"

and “carboxylic acids and derivatives” (Figure 4-G), which were enriched prominently to “sphingolipid metabolism”, “purine Metabolism”, “methionine metabolism”, “selenoamino acid metabolism”, “bile acid biosynthesis”, “taurine and hypotaurine metabolism”, “retinol metabolism” and “betaine metabolism” (Table S6, Figure 4-H). The differential metabolites distinct in IS-FEMALE *vs*. IB-FEMALE were classified prominently into “glycerophospholipids”, “carboxylic acids and derivatives”, “fatty acyls”, “organonitrogen compounds” and “purine nucleosides” (Figure 4-I), which were enriched prominently to “retinol metabolism”, “purine metabolism”, “glutamate metabolism”, “alpha linolenic acid and linoleic acid metabolism” and “warburg effect” (Table S7, Figure 4-J).

Altered metabolic pathways and their biological significance

The pathway analysis performed using *MetaboAnalyst* for the involved biological pathways and biological roles of the above differentially expressed metabolites determined that the perturbed metabolic pathways reporting lower p-values and higher pathway impact in male worms from SCID mice compared with those from BALB/c mice mainly included arachidonic acid metabolism, alpha-linolenic acid metabolism, taurine and hypotaurine metabolism, sphingolipid metabolism, glycerophospholipid metabolism, and etc (Table S8, Figure S2-A). Meanwhile, more affected metabolic pathways in female worms from SCID mice compared with those from BALB/c mice were determined, and the top 5 metabolic pathways included biotin metabolism, tryptophan metabolism, purine metabolism, glyoxylate and dicarboxylate metabolism, tyrosine metabolism (Table S9, Figure S2-B).

Metabolic pathways analysis based on the common differential metabolites between IS-MALE *vs*. IB-MALE and IS-FEMALE *vs*. IB-FEMALE found that tryptophan metabolism,

aminoacyl-tRNA biosynthesis, purine metabolism, glycerophospholipid metabolism, arachidonic acid metabolism and alpha-linolenic acid metabolism were commonly perturbed in both male and female worms from SCID mice compared with BALB/c mice (Table S10, Figure S2-C). Metabolic pathways analysis based on the differential metabolites distinct in IS-MALE *vs*. IB-MALE found their involved metabolic pathways included sphingolipid metabolism, glycerophospholipid metabolism, taurine and hypotaurine metabolism, purine metabolism, glycine/serine/threonine metabolism, cysteine and methionine metabolism, cyanoamino acid metabolism, glyoxylate and dicarboxylate metabolism and aminoacyl-tRNA biosynthesis (Table S11, Figure S2-D). More metabolic pathways based on the differential metabolites distinct in IS-FEMALE *vs*. IB-FEMALE were found and the top five metabolic pathways were arachidonic acid metabolism, glycerophospholipid metabolism, glycosylphosphatidylinositol (GPI)-anchor biosynthesis, alpha-linolenic acid metabolism and glyoxylate and dicarboxylate metabolism (Table S12, Figure S2-E).

Discussion

The schistosomes exhibit dioecy and have a complex life cycle transforming between their definitive hosts - mammals and their intermediate hosts - snails. Every mature female worm lay hundreds to thousands of eggs per day, which is a complex metabolic process such as the fatty acid oxidation, etc [36]. A certain part of the released eggs are deposited in the liver, intestinal wall and other tissues, which are the key pathogenic factor to severe schistosomiasis. So, it is a feasible approach to control schistosomiasis by interfering with the growth, development and oviposition of schistosomes in their hosts. It has been already discovered that schistosome showed retarded growth, development and reproduction in the

immunodeficient mammalian hosts, and exerted attenuated pathogenesis with decreased egg-laying and granulomas formation in the hosts. However, very limited knowledge about the molecular mechanism behind the distinct phenotypic abnormalities of schistosomes in their immunodeficient hosts is accessible. For the abnormal schistosomes in immunodeficient hosts, e.g. SCID mice, we believe it is a perfect model by comparative omics to identify molecules potentially participate in the regulation of growth and development of schistosomes when compared with those with normal growth and development in immunocompetent mice, e.g. BALB/c mice. In this study, therefore, an untargeted LC-MS/MS-based high-resolution metabolomic investigation was performed and distinct bio-signatures in the metabolic profiles of male and female *S. japonicum* worms in SCID mice were found when compared with those in BALB/c mice, respectively.

In the results, multivariate analysis by both PCA and PLS-DA found larger differences between IS-FEMALE and IB-FEMALE than that between IS-MALE and IB-MALE. This indicates the female schistosome worms were affected more severely than the male worms in SCID mice, which was verified by the subsequent finding that more differential metabolites were acquired in IS-FEMALE *vs*. IB-FEMALE than IS-MALE *vs*. IB-MALE. This is expectable and reasonable as the growth and development of female worms were affected by male worms as well as the host's factors, i.e. the sexual maturation of female worms depends on pairing with male worms. In the list of differential metabolites of IS-FEMALE *vs*. IB-FEMALE, retinyl ester was the only up-regulated metabolite of female worms from SCID mice, which was enriched in "retinol metabolism". Numerous researches reported that the retinol metabolism, in which retinyl ester is involved, regulates gametogenesis and reproduction by the product transcriptionally active retinoic acid [37-41]. In the retinol metabolism pathway of

animals, all-trans retinyl esters in the body is formed by transferring a fatty acyl moiety from the sn-1 position of membrane phosphatidyl choline (e.g. PC(22:6/20:1), traditionally named as lecithin) to all-trans-retinol under the catalysis of lecithin:retinol acyltransferase (LRAT), whose orthologue in *Schistosoma* is diacylglycerol O-acyltransferase (DGAT). Unesterified all-trans-retinol, which could be reversibly liberated from all-trans retinyl esters stores through the action of a retinyl ester hydrolase (REH), is oxidized by one retinol dehydrogenase (RDH) to all-trans-retinal, which can be also reversibly transformed to all-trans-retinol by the catalysis of retinal reductase (RALR). All-trans-retinal, which is originally derived from the decomposition of proretinoid carotenoids such as dietary β-carotene, is then irreversibly oxidized by one retinal dehydrogenase (RALDH) to form transcriptionally active all-trans retinoic acid [42]. LRAT is a key enzyme involved in retinoids homeostasis and is regulated in response to retinoic acid, and it can also negatively regulate retinoic acid biosynthesis by diverting retinol away from oxidative activation [42]. Therefore, we speculate higher level of retinyl ester found in the female worms from SCID mice logically means lower level of lecithin, which should be consumed to synthesize retinyl ester. What was consistent with this inference was that PC(22:6/20:1) (HMDB0008735, with full name as 1-docosahexaenoyl-2-eicosenoyl-sn-glycero-3-phosphocholine, or traditional name as lecithin) happened to be decreased in the female worms from SCID mice when compared with those from BALB/c mice in the results (Figure 5). So, we speculated that the accumulated retinyl ester in the female worms from SCID mice resulted in insufficient formation of the active retinoic acid. It is known that retinoic acid is the meiosis-inducing factor in both sexes, and inhibition of retinoic acid biosynthesis would markedly suppresses gametogenesis [37-41, 43-54]. In addition, overexpression of LRAT will favor retinyl ester formation, which would disrupt retinol homeostasis and interrupt

the ability of downstream metabolites to regulate transcription of genes involved in various biological processes. Various cancer cells have been found to have low levels of LRAT and retinyl ester levels. Overexpression of LRAT or increased level of retinyl esters themselves makes cells more sensitive to carcinogen-induced tumorigenesis and leison [55, 56]. So, insufficient retinoic acid biosynthesis due to prevailing retinyl ester formation could be a significant cause for the retarded development and declined fertility appeared in female worms from SCID mice in this study. Meanwhile, lecithin is a source of several active compounds: choline and its metabolites are needed for several physiological purposes, including cell membrane signaling and cholinergic neurotransmission during growth and reproduction [57, 58]. So, excessive lecithin consumption in retinyl ester formation probably lead to worse effect in the development and reproduction of schistosomes besides insufficient retinoic acid biosynthesis. In contrast, however, an extremely higher level of lecithin was detected in the male worms from SCID mice than BALB/c mice, with a relative fold as high as 17.53 for IS-MALE *vs*. IB-MALE. It is known that the schistosomes are dioecious trematodes, and embracing with the male worm by residing in the male's gynaecophoric channel is crucial for the female worm to grow and sexually mature [59]. So, we speculated that insufficient interaction between the male and female worms, which manifested as decreased percent of worm pairs reported in our previous research [12], resulted in insufficient material exchange or transfer between them, such as the probable lecithin transfer from male worms to female worms. Similar alterations in fatty acyls, glycerophospholipids, purine nucleosides, imidazopyrimidines and indoles and derivatives were detected in both male and female worms from SCID mice when compared with BALB/c mice, but opposite alterations were detected in carboxylic acids and derivatives (Figure 4-A, C, E). Common decrease in

glycerophospholipids synthesis with lysoPCs, lysoPEs and PCs as the top three alter metabolites, one of the main functions of which is to serve as a structural component of biological membranes [60, 61], indicated attenuated parasite establishment with smaller body size and attenuated reproduction due to potentially deficient glycerophospholipids in worms from SCID mice. Sphingolipids are commonly believed to protect the cell surface against harmful environmental factors [62, 63], and arachidonic acid is involved in cellular signaling as a lipid second messenger as a polyunsaturated fatty acid present in the phospholipids [64, 65]. Their involved metabolic pathways of important biological significance such as sphingolipid metabolism and arachidonic acid metabolism were also found abnormal with decreased sphingolipids in male and arachidonic acid in female worms from SCID mice, respectively, which may be also associated with the developmentally stunted worms.

Furthermore, the level of tryptophan, an essential amino acid, was found decreased in both male and female worms from SCID mice. Tryptophan acts as a precursor for the synthesis of the neurotransmitters melatonin and serotonin and then, any reduction in tryptophan will lead to a number of conditions or diseases e.g. dermatitis and psychiatric symptom – depression in animals, it seems in this study to contribute to inhibiting of the growth and reproduction of worms finally [66-71]. Ergothioneine is a product of plant origin that accumulates in animal tissues and a naturally occurring metabolite of histidine that has antioxidant properties though its physiological role in vivo is undetermined [72]. Decrease of ergothioneine was found in female worms from SCID mice, which indicated increased susceptibility to oxidative damage in them [73-75].

In conclusion, the identified differential metabolites and their involved metabolic pathways are likely associated with the abnormalities in growth and development of *S. japonicum* worms

in SCID mice when compared with those in BALB/c mice. Differential alterations in metabolic profiles between male and female worms from SCID mice when compared with BALB/c mice indicated the degree and mechanism of the influence the host on male and female worms were different. Our data has demonstrated the great ability of LC-MS/MS-based metabolomics to detect a broad range of differential metabolites in worms that strongly distinguished between their different hosts - the SCID mice and BALB/c mice. The above mentioned differential metabolites, together with the others not mentioned here in particular, need further verification and investigations for their underlying mechanisms in the regulation of growth and development of schistosome. This will, as a result, greatly facilitate the discovery of new drugs and vaccines against schistosome and schistosomiasis.

Supporting Information

Figure legends

Figure 1. Differential metabolic profiles of male and female *S. japonicum* worms between SCID mice and BALB/c mice at 35 days post infection. Principal component analysis (PCA) score scatter plots of metabolites obtained from LC-MS/MS fingerprints in ESI+ (A) and ESI- mode (B). Partial least-squares discriminant analysis (PLS-DA) separating metabolites of the four groups of worms and QC sample in ESI+ (C) and ESI- mode (D). IB-MALE denotes the male worms from BALB/c mice, which are marked with green plus sign. IB-FEMALE denotes the female worms from BALB/c mice, which are marked with red triangles. IS-MALE denotes the male worms from SCID mice, which are marked with blue diamonds. IS-FEMALE denotes the female worms from SCID mice, which are marked with purple cross. QC denotes the quality control samples, which are marked with pink triangles.

Figure 2. Discrimination between the *S. japonicum* worms from SCID mice and those from BALB/c mice with *S. japonicum* infection for 35 days based on ESI+ and ESI- mode-derived metabolic phenotypes and heatmaps of the differential metabolites between the compared groups.

A-B: Orthogonal partial least-squares discriminant analysis (OPLS-DA) score plots in ESI+ mode (A) and ESI- mode (B) for comparison between male worms from SCID mice and those from BALB/c mice (IB-MALE denotes the male worms from BALB/c mice and IS-MALE denotes the male worms from SCID mice). **C**: Heatmap of the differential metabolites between male worms from SCID mice and those from BALB/c mice. **D-E**: Orthogonal partial least-

squares discriminant analysis (OPLS-DA) score plots in ESI+ mode (A) and ESI- mode (B) for comparison between female worms from SCID mice and those from BALB/c mice (IB-FEMALE denotes the female worms from BALB/c mice and IS-FEMALE denotes the female worms from SCID mice). **F**: Heatmap of the differential metabolites between female worms from SCID mice and those from BALB/c mice. For the heatmaps, normalized signal intensities (log2 transformed and row adjustment) are visualized as a color spectrum and the scale from least abundant to highest ranges is from -3.0 to 3.0 as shown in the colorbar. Green indicates decreased expression, whereas red indicates increased expression of the detected metabolites between compared groups.

Figure 3. Comparison of metabolomics between the *S. japonicum* worms from SCID mice and those from BALB/c mice with *S. japonicum* infection for 35 days heatmaps of their differential metabolites.

A: Differential metabolites across comparison groups showing unique and common metabolites between IS-MALE vs. IB-MALE and IS-FEMALE vs. IB-FEMALE. Venn diagram displays comparatively the differentially expressed metabolites. All the differentially expressed metabolites are clustered into two comparison groups represented by two circles. The sum of all the figures in one circle represents the number of differentially expressed metabolites in one comparison group (e.g. IS-MALE *vs*. IB-MALE). The overlapping part of the two circles represents the number of differentially expressed metabolites shared between the two comparison groups. The single-layer part represents the number of metabolites distinctly found in a certain comparison group. **B-C**: Heatmap of the common (B) and distinct (C is for male worms and D is for female worms) differential metabolites between male worms and

female worms. For the heatmaps, normalized signal intensities (log2 transformed and row adjustment) are visualized as a color spectrum and the scale from least abundant to highest ranges is from -3.0 to 3.0 as shown in the colorbar. Green indicates decreased expression, whereas red indicates increased expression of the detected metabolites between compared groups.

Figure 4. Enrichment analysis of the differential metabolites across comparison groups. A: Top 8 enriched metabolite terms of the differentially expressed metabolites of IS-MALE vs. IB-MALE. The bars on x-axis represent the number of metabolites for the chemical classes mentioned on the y-axis. **B**: Enriched metabolite sets of the differentially expressed metabolites of IS-MALE vs. IB-MALE. **C**: Top 11 enriched metabolite terms of the differentially expressed metabolites of IS-FEMALE vs. IB-FEMALE. **D**: Enriched metabolite sets of the differentially expressed metabolites of IS-FEMALE vs. IB-FEMALE. **E**: Enriched metabolite terms of the common differentially expressed metabolites between IS-MALE vs. IB-MALE and IS-FEMALE vs. IB-FEMALE. **F**: Enriched metabolite sets of the differentially expressed metabolites between IS-MALE vs. IB-MALE and IS-FEMALE vs. IB-FEMALE. **G**: Enriched metabolite terms of the differentially expressed metabolites distinct in IS-MALE vs. IB-MALE. **H**: Enriched metabolite sets of the differentially expressed metabolites distinct in IS-MALE vs. IB-MALE. **I**: Enriched metabolite terms of the differentially expressed metabolites distinct in IS-FEMALE vs. IB-FEMALE. **J**: Enriched metabolite sets of the differentially expressed metabolites distinct in IS-FEMALE vs. IB-FEMALE.

Figure 5. The metabolism of retinoids Retinal can be originally formed by the cleavage of proretinoid carotenoids such as beta-carotene by the enzyme BCMO1 (not shown here). Retinol is formed by the reversible reduction of retinal by one of the retinal reductase family members. The enzyme lecithin:retinol acyl-transferase (LRAT) (with an orthologue gene called diacylglycerol O-acyltransferase (DGAT) in *Schistosoma japonicum*) synthesizes retinyl esters by transferring a fatty acyl moiety from the sn-1 position of membrane phosphatidyl choline such as lecithin (PC(22:6/20:1)) to retinol. Unesterified retinol is liberated from retinyl ester stores by the catalysis of a retinyl ester hydrolase (REH). Retinol is oxidized by catalysis of one retinol dehydrogenase (RDH) to retinal, which is then irreversibly oxidized by one retinal dehydrogenase (RALDH) to form transcriptionally active retinoic acid. Retinoic acid is finally oxidized/catabolized to more water-soluble hydroxy- and oxo- forms by one of several cytochrome P450 enzyme family members.

Figure S1. The stacked total ion chromatograms of QC sample. A: The stacked total ion chromatogram of QC sample in ESI+ mode. **B**: The stacked total ion chromatogram of QC sample in ESI- mode. The bars on x-axis represent the retention time (0~15 min) and the bars on y-axis represent the total ion strength.

Figure S2. Summary of the aberrant metabolic pathways based on the significantly altered metabolites of the comparison groups as analyzed by Pathway Analysis of *MetaboAnalyst*. Plots show the matched pathways depicted according to *P*-value from pathway enrichment analysis and pathway impact score from pathway topology analysis. **A**: Enriched metabolic pathways based on the differential

metabolites between IS-MALE vs. IB-MALE. **B**: Enriched metabolic pathways based on the differential serum metabolites between IS-FEMALE vs. IB-FEMALE. **C**: Enriched metabolic pathways based on the differential metabolites common in IS-MALE vs. IB-MALE and IS-FEMALE vs. IB-FEMALE. **D**: Enriched metabolic pathways based on the differential metabolites distinct in IS-MALE vs. IB-MALE. **E**: Enriched metabolic pathways based on the differential metabolites distinct in IS-FEMALE vs. IB-FEMALE. Color gradient and circle size indicate the significance of the pathway ranked by *P*-value (yellow: higher *P*-values and red: lower *P*-values) and pathway impact score (the larger the circle the higher the impact score), respectively. Significantly affected pathways with low *P*-value and high pathway impact score are identified by name.

Supporting table legends

Table S1. Differential metabolites of male worms from SCID mice compared with those from BALB/c mice. This table contains a list of the differential metabolites between male worms from SCID mice and male worms from BALB/c mice.
(DOCX)

Table S2. Differential metabolites of female worms from SCID mice compared with those from BALB/c mice. This table contains a list of the differential metabolites between female worms from SCID mice and female worms from BALB/c mice.
(DOCX)

Table S3. Metabolite set enrichment of the differential metabolites of male worms between SCID mice and BALB/c mice. Metabolite sets are enriched of the differential metabolites between male worms from SCID mice and male worms from BALB/c mice.
(DOCX)

Table S4. Metabolite set enrichment of the differential metabolites of female worms between SCID mice and BALB/c mice. Metabolite sets are enriched of the differential metabolites between female worms from SCID mice and female worms from BALB/c mice.
(DOCX)

Table S5. Metabolite set enrichment of the common differential metabolites in male and female worms from SCID mice. Metabolite sets are enriched of the common differential metabolites between male worms and female worms from SCID mice compared with those from BALB/c mice.
(DOCX)

Table S6. Metabolite set enrichment of the male worm-specific differential metabolites between SCID mice and BALB/c mice. Metabolite sets are enriched of the male worm-specific differential metabolites between SCID mice and BALB/c mice.
(DOCX)

Table S7. Metabolite set enrichment of the female worm-specific differential metabolites of those between SCID mice and BALB/c mice. Metabolite sets are enriched of the female worm-specific differential metabolites between SCID mice and BALB/c mice.
(DOCX)

Table S8. Pathway analysis of the differential metabolites of male worms between SCID mice and BALB/c mice. This list contains the enriched metabolic pathways of the differential metabolites of male worms between SCID mice and BALB/c mice.
(DOCX)

Table S9. Pathway analysis of the differential metabolites of female worms between SCID mice and BALB/c mice. This list contains the enriched metabolic pathways of the differential metabolites of female worms between SCID mice and BALB/c mice.
(DOCX)

Table S10. Pathway analysis of the common differential metabolites in male and female worms from SCID mice. This list contains the enriched metabolic pathways of the common differential metabolites between male worms and female worms from SCID mice compared with those from BALB/c mice.
(DOCX)

Table S11. Pathway analysis of the male worm-specific differential metabolites between SCID mice and BALB/c mice. This list contains the enriched metabolic pathways of the male worm-specific differential metabolites between SCID mice and BALB/c mice.
(DOCX)

Table S12. Pathway analysis of the female worm-specific differential metabolites between SCID mice and BALB/c mice. This list contains the enriched metabolic pathways of the female worm-specific differential metabolites between SCID mice and BALB/c mice.
(DOCX)

References

1. Gray DJ, McManus DP, Li Y, Williams GM, Bergquist R, Ross AG. Schistosomiasis elimination: lessons from the past guide the future. The Lancet Infectious diseases. 2010;10(10):733-6. doi: 10.1016/S1473-3099(10)70099-2. PubMed PMID: 20705513.

2. WHO. Schistosomiasis: number of people receiving preventive chemotherapy in 2012. Releve epidemiologique hebdomadaire. 2014;89(2):21-8. PubMed PMID: 24446558.

3. Ross AG, Bartley PB, Sleigh AC, Olds GR, Li Y, Williams GM, et al. Schistosomiasis. The New England journal of medicine. 2002;346(16):1212-20. doi: 10.1056/NEJMra012396. PubMed PMID: 11961151.

4. Saule P, Adriaenssens E, Delacre M, Chassande O, Bossu M, Auriault C, et al. Early variations of host thyroxine and interleukin-7 favor Schistosoma mansoni development. The Journal of parasitology. 2002;88(5):849-55. doi: 10.1645/0022-3395(2002)088[0849:EVOHTA]2.0.CO;2. PubMed PMID: 12435119.

5. de Mendonca RL, Escriva H, Bouton D, Laudet V, Pierce RJ. Hormones and nuclear receptors in schistosome development. Parasitology today. 2000;16(6):233-40. PubMed PMID: 10827428.

6. Davies SJ, Lim KC, Blank RB, Kim JH, Lucas KD, Hernandez DC, et al. Involvement of TNF in limiting liver pathology and promoting parasite survival during schistosome infection. International journal for parasitology. 2004;34(1):27-36. PubMed PMID: 14711587; PubMed Central PMCID: PMC2859728.

7. Halton DW. Nutritional adaptations to parasitism within the platyhelminthes. International journal for parasitology. 1997;27(6):693-704. PubMed PMID: 9229252.

8. Hernandez DC, Lim KC, McKerrow JH, Davies SJ. Schistosoma mansoni: sex-specific

modulation of parasite growth by host immune signals. Experimental parasitology. 2004;106(1-2):59-61. doi: 10.1016/j.exppara.2004.01.003. PubMed PMID: 15013791; PubMed Central PMCID: PMC2891232.

9. You H, Gobert GN, Cai P, Mou R, Nawaratna S, Fang G, et al. Suppression of the Insulin Receptors in Adult Schistosoma japonicum Impacts on Parasite Growth and Development: Further Evidence of Vaccine Potential. PLoS neglected tropical diseases. 2015;9(5):e0003730. doi: 10.1371/journal.pntd.0003730. PubMed PMID: 25961574; PubMed Central PMCID: PMC4427307.

10. Lamb EW, Walls CD, Pesce JT, Riner DK, Maynard SK, Crow ET, et al. Blood fluke exploitation of non-cognate CD4+ T cell help to facilitate parasite development. PLoS pathogens. 2010;6(4):e1000892. doi: 10.1371/journal.ppat.1000892. PubMed PMID: 20442785; PubMed Central PMCID: PMC2861709.

11. Blank RB, Lamb EW, Tocheva AS, Crow ET, Lim KC, McKerrow JH, et al. The common gamma chain cytokines interleukin (IL)-2 and IL-7 indirectly modulate blood fluke development via effects on CD4+ T cells. The Journal of infectious diseases. 2006;194(11):1609-16. doi: 10.1086/508896. PubMed PMID: 17083048; PubMed Central PMCID: PMC2853799.

12. Tang H, Ming Z, Liu R, Xiong T, Grevelding CG, Dong H, et al. Development of adult worms and granulomatous pathology are collectively regulated by T- and B-cells in mice infected with Schistosoma japonicum. PloS one. 2013;8(1):e54432. doi: 10.1371/journal.pone.0054432. PubMed PMID: 23349889; PubMed Central PMCID: PMC3551845.

13. Cheng YL, Song WJ, Liu WQ, Lei JH, Mo HM, Ruppel A, et al. The effects of T cell deficiency on the development of worms and granuloma formation in mice infected with Schistosoma japonicum. Parasitology research. 2008;102(6):1129-34. doi: 10.1007/s00436-008-0880-0.

PubMed PMID: 18246371.

14. Davies SJ, Grogan JL, Blank RB, Lim KC, Locksley RM, McKerrow JH. Modulation of blood fluke development in the liver by hepatic CD4+ lymphocytes. Science. 2001;294(5545):1358-61. doi: 10.1126/science.1064462. PubMed PMID: 11701932.

15. Amiri P, Locksley RM, Parslow TG, Sadick M, Rector E, Ritter D, et al. Tumour necrosis factor alpha restores granulomas and induces parasite egg-laying in schistosome-infected SCID mice. Nature. 1992;356(6370):604-7. doi: 10.1038/356604a0. PubMed PMID: 1560843.

16. Sengupta A, Ghosh S, Sharma S, Sonawat HM. 1H NMR metabonomics indicates continued metabolic changes and sexual dimorphism post-parasite clearance in self-limiting murine malaria model. PloS one. 2013;8(6):e66954. doi: 10.1371/journal.pone.0066954. PubMed PMID: 23826178; PubMed Central PMCID: PMC3691208.

17. Wang Y, Utzinger J, Saric J, Li JV, Burckhardt J, Dirnhofer S, et al. Global metabolic responses of mice to Trypanosoma brucei brucei infection. Proceedings of the National Academy of Sciences of the United States of America. 2008;105(16):6127-32. doi: 10.1073/pnas.0801777105. PubMed PMID: 18413599; PubMed Central PMCID: PMC2329718.

18. Zhou CX, Zhou DH, Elsheikha HM, Liu GX, Suo X, Zhu XQ. Global Metabolomic Profiling of Mice Brains following Experimental Infection with the Cyst-Forming Toxoplasma gondii. PloS one. 2015;10(10):e0139635. doi: 10.1371/journal.pone.0139635. PubMed PMID: 26431205; PubMed Central PMCID: PMC4592003.

19. Garcia-Perez I, Whitfield P, Bartlett A, Angulo S, Legido-Quigley C, Hanna-Brown M, et al. Metabolic fingerprinting of Schistosoma mansoni infection in mice urine with capillary electrophoresis. Electrophoresis. 2008;29(15):3201-6. doi: 10.1002/elps.200800031. PubMed

PMID: 18633941.

20. Thompson SN. Metabolic integration during the host associations of multicellular animal endoparasites. Comparative biochemistry and physiology B, Comparative biochemistry. 1985;81(1):21-42. PubMed PMID: 3893873.

21. Li JV, Holmes E, Saric J, Keiser J, Dirnhofer S, Utzinger J, et al. Metabolic profiling of a Schistosoma mansoni infection in mouse tissues using magic angle spinning-nuclear magnetic resonance spectroscopy. International journal for parasitology. 2009;39(5):547-58. doi: 10.1016/j.ijpara.2008.10.010. PubMed PMID: 19068218.

22. O'Sullivan C, Fried B, Sherma J. Metabolic profiling of Echinostoma caproni and Schistosoma mansoni in their definitive and intermediate hosts. Acta parasitologica. 2013;58(1):1-5. doi: 10.2478/s11686-013-0104-3. PubMed PMID: 23377904.

23. Bowman IB, Grant PT, Kermack WO. The metabolism of Plasmodium berghei, the malaria parasite of rodents. I. The preparation of the erythrocytic form of P. berghei separated from the host cell. Experimental parasitology. 1960;9:131-6. PubMed PMID: 13803493.

24. Hellerman L, Bovarnick MR, Porter CC. Metabolism of the malarial parasite; action of antimalarial agents upon separated Plasmodium lophurae and upon certain isolated enzyme systems. Federation proceedings. 1946;5:400-5. PubMed PMID: 20999489.

25. Adebayo AS, Mundhe SD, Awobode HO, Onile OS, Agunloye AM, Isokpehi RD, et al. Metabolite profiling for biomarkers in Schistosoma haematobium infection and associated bladder pathologies. PLoS neglected tropical diseases. 2018;12(4):e0006452. doi: 10.1371/journal.pntd.0006452. PubMed PMID: 29708967.

26. Teng R, Junankar PR, Bubb WA, Rae C, Mercier P, Kirk K. Metabolite profiling of the intraerythrocytic malaria parasite Plasmodium falciparum by (1)H NMR spectroscopy. NMR in

biomedicine. 2009;22(3):292-302. doi: 10.1002/nbm.1323. PubMed PMID: 19021153.

27. Legido-Quigley C. Metabolite-biomarker investigations in the life cycle of and infection with Schistosoma. Parasitology. 2010;137(9):1425-35. doi: 10.1017/S0031182010000545. PubMed PMID: 20550753.

28. Zhou CX, Zhou DH, Elsheikha HM, Zhao Y, Suo X, Zhu XQ. Metabolomic Profiling of Mice Serum during Toxoplasmosis Progression Using Liquid Chromatography-Mass Spectrometry. Scientific reports. 2016;6:19557. doi: 10.1038/srep19557. PubMed PMID: 26785939; PubMed Central PMCID: PMC4726199.

29. Wang Y, Holmes E, Nicholson JK, Cloarec O, Chollet J, Tanner M, et al. Metabonomic investigations in mice infected with Schistosoma mansoni: an approach for biomarker identification. Proceedings of the National Academy of Sciences of the United States of America. 2004;101(34):12676-81. doi: 10.1073/pnas.0404878101. PubMed PMID: 15314235; PubMed Central PMCID: PMC515115.

30. Want EJ, Masson P, Michopoulos F, Wilson ID, Theodoridis G, Plumb RS, et al. Global metabolic profiling of animal and human tissues via UPLC-MS. Nature protocols. 2013;8(1):17-32. doi: 10.1038/nprot.2012.135. PubMed PMID: 23222455.

31. Want EJ, Wilson ID, Gika H, Theodoridis G, Plumb RS, Shockcor J, et al. Global metabolic profiling procedures for urine using UPLC-MS. Nature protocols. 2010;5(6):1005-18. doi: 10.1038/nprot.2010.50. PubMed PMID: 20448546.

32. Cui L, Zheng D, Lee YH, Chan TK, Kumar Y, Ho WE, et al. Metabolomics Investigation Reveals Metabolite Mediators Associated with Acute Lung Injury and Repair in a Murine Model of Influenza Pneumonia. Scientific reports. 2016;6:26076. doi: 10.1038/srep26076. PubMed PMID: 27188343; PubMed Central PMCID: PMC4870563.

33. Xia J, Sinelnikov IV, Han B, Wishart DS. MetaboAnalyst 3.0--making metabolomics more meaningful. Nucleic acids research. 2015;43(W1):W251-7. doi: 10.1093/nar/gkv380. PubMed PMID: 25897128; PubMed Central PMCID: PMC4489235.

34. Chong J, Soufan O, Li C, Caraus I, Li S, Bourque G, et al. MetaboAnalyst 4.0: towards more transparent and integrative metabolomics analysis. Nucleic acids research. 2018;46(W1):W486-W94. doi: 10.1093/nar/gky310. PubMed PMID: 29762782; PubMed Central PMCID: PMC6030889.

35. Xia J, Wishart DS. Using MetaboAnalyst 3.0 for Comprehensive Metabolomics Data Analysis. Current protocols in bioinformatics. 2016;55:14 0 1- 0 91. doi: 10.1002/cpbi.11. PubMed PMID: 27603023.

36. Pearce EJ, Huang SC. The metabolic control of schistosome egg production. Cellular microbiology. 2015;17(6):796-801. doi: 10.1111/cmi.12444. PubMed PMID: 25850569; PubMed Central PMCID: PMC4867551.

37. Koubova J, Menke DB, Zhou Q, Capel B, Griswold MD, Page DC. Retinoic acid regulates sex-specific timing of meiotic initiation in mice. Proceedings of the National Academy of Sciences of the United States of America. 2006;103(8):2474-9. doi: 10.1073/pnas.0510813103. PubMed PMID: 16461896; PubMed Central PMCID: PMC1413806.

38. Alsop D, Matsumoto J, Brown S, Van Der Kraak G. Retinoid requirements in the reproduction of zebrafish. General and comparative endocrinology. 2008;156(1):51-62. doi: 10.1016/j.ygcen.2007.11.008. PubMed PMID: 18158153.

39. Kim YK, Wassef L, Hamberger L, Piantedosi R, Palczewski K, Blaner WS, et al. Retinyl ester formation by lecithin: retinol acyltransferase is a key regulator of retinoid homeostasis in mouse embryogenesis. The Journal of biological chemistry. 2008;283(9):5611-21. doi:

10.1074/jbc.M708885200. PubMed PMID: 18093970; PubMed Central PMCID: PMC3771510.

40. Chung SS, Wolgemuth DJ. Role of retinoid signaling in the regulation of spermatogenesis. Cytogenetic and genome research. 2004;105(2-4):189-202. doi: 10.1159/000078189. PubMed PMID: 15237207; PubMed Central PMCID: PMC3803148.

41. Amory JK, Muller CH, Shimshoni JA, Isoherranen N, Paik J, Moreb JS, et al. Suppression of spermatogenesis by bisdichloroacetyldiamines is mediated by inhibition of testicular retinoic acid biosynthesis. Journal of andrology. 2011;32(1):111-9. doi: 10.2164/jandrol.110.010751. PubMed PMID: 20705791; PubMed Central PMCID: PMC3370679.

42. O'Byrne SM, Blaner WS. Retinol and retinyl esters: biochemistry and physiology. Journal of lipid research. 2013;54(7):1731-43. doi: 10.1194/jlr.R037648. PubMed PMID: 23625372; PubMed Central PMCID: PMC3679378.

43. Anderson EL, Baltus AE, Roepers-Gajadien HL, Hassold TJ, de Rooij DG, van Pelt AM, et al. Stra8 and its inducer, retinoic acid, regulate meiotic initiation in both spermatogenesis and oogenesis in mice. Proceedings of the National Academy of Sciences of the United States of America. 2008;105(39):14976-80. doi: 10.1073/pnas.0807297105. PubMed PMID: 18799751; PubMed Central PMCID: PMC2542382.

44. Bowles J, Knight D, Smith C, Wilhelm D, Richman J, Mamiya S, et al. Retinoid Signaling Determines Germ Cell Fate in Mice. Science. 2006;312(5773):596-600.

45. Doyle TJ, Braun KW, McLean DJ, Wright RW, Griswold MD, Kim KH. Potential functions of retinoic acid receptor A in Sertoli cells and germ cells during spermatogenesis. Annals of the New York Academy of Sciences. 2007;1120:114-30. doi: 10.1196/annals.1411.008. PubMed PMID: 17905941.

46. Duester G. Retinoid signaling in control of progenitor cell differentiation during mouse

development. Seminars in cell & developmental biology. 2013;24(10-12):694-700. doi: 10.1016/j.semcdb.2013.08.001. PubMed PMID: 23973941; PubMed Central PMCID: PMC3849222.

47. Kim KH, Griswold MD. The regulation of retinoic acid receptor mRNA levels during spermatogenesis. Molecular endocrinology. 1990;4(11):1679-88. doi: 10.1210/mend-4-11-1679. PubMed PMID: 2177839.

48. Liu Z, Sun Y, Jiang Y, Qian Y, Chen S, Gao S, et al. Follicle-stimulating hormone (FSH) promotes retinol uptake and metabolism in the mouse ovary. Reproductive biology and endocrinology : RB&E. 2018;16(1):52. doi: 10.1186/s12958-018-0371-9. PubMed PMID: 29803227; PubMed Central PMCID: PMC5970539.

49. Nicholls PK, Harrison CA, Rainczuk KE, Wayne Vogl A, Stanton PG. Retinoic acid promotes Sertoli cell differentiation and antagonises activin-induced proliferation. Molecular and cellular endocrinology. 2013;377(1-2):33-43. doi: 10.1016/j.mce.2013.06.034. PubMed PMID: 23831638.

50. Nourashrafeddin S, Hosseini Rashidi B. Gonadotropin Regulation of Retinoic Acid Activity in the Testis. Acta medica Iranica. 2018;56(1):34-42. PubMed PMID: 29436793.

51. Paik J, Haenisch M, Muller CH, Goldstein AS, Arnold S, Isoherranen N, et al. Inhibition of retinoic acid biosynthesis by the bisdichloroacetyldiamine WIN 18,446 markedly suppresses spermatogenesis and alters retinoid metabolism in mice. The Journal of biological chemistry. 2014;289(21):15104-17. doi: 10.1074/jbc.M113.540211. PubMed PMID: 24711451; PubMed Central PMCID: PMC4031560.

52. Pradhan A, Olsson PE. Inhibition of retinoic acid synthesis disrupts spermatogenesis and fecundity in zebrafish. General and comparative endocrinology. 2015;217-218:81-91. doi:

10.1016/j.ygcen.2015.02.002. PubMed PMID: 25687389.

53. Teletin M, Vernet N, Ghyselinck NB, Mark M. Roles of Retinoic Acid in Germ Cell Differentiation. Current topics in developmental biology. 2017;125:191-225. doi: 10.1016/bs.ctdb.2016.11.013. PubMed PMID: 28527572.

54. Yu M, Yu P, Leghari IH, Ge C, Mi Y, Zhang C. RALDH2, the enzyme for retinoic acid synthesis, mediates meiosis initiation in germ cells of the female embryonic chickens. Amino acids. 2013;44(2):405-12. doi: 10.1007/s00726-012-1343-6. PubMed PMID: 22733143.

55. Ghosh R. Lecithin: Retinol acyltransferase and retinyl esters—is balance the essence in carcinogenesis? Cancer Biology & Therapy. 2014;8(13):1226-7. doi: 10.4161/cbt.8.13.8902.

56. Tang XH, Su D, Albert M, Scognamiglio T, Gudas LJ. Overexpression of lecithin:retinol acyltransferase in the epithelial basal layer makes mice more sensitive to oral cavity carcinogenesis induced by a carcinogen. Cancer Biol Ther. 2009;8(13):1212-3. PubMed PMID: 19471114; PubMed Central PMCID: PMC2882701.

57. Attia YA, Hussein AS, Tag El-Din AE, Qota EM, Abed El-Ghany AI, El-Sudany AM. Improving productive and reproductive performance of dual-purpose crossbred hens in the tropics by lecithin supplementation. Tropical animal health and production. 2009;41(4):461-75. doi: 10.1007/s11250-008-9209-3. PubMed PMID: 18661247.

58. Attia YA, Kamel KI. Semen quality, testosterone, seminal plasma biochemical and antioxidant profiles of rabbit bucks fed diets supplemented with different concentrations of soybean lecithin. Animal : an international journal of animal bioscience. 2012;6(5):824-33. doi: 10.1017/S1751731111002229. PubMed PMID: 22558930.

59. Gryseels B, Polman K, Clerinx J, Kestens L. Human schistosomiasis. Lancet. 2006;368(9541):1106-18. doi: 10.1016/S0140-6736(06)69440-3. PubMed PMID: 16997665.

60. Farooqui AA, Horrocks LA, Farooqui T. Glycerophospholipids in brain: their metabolism, incorporation into membranes, functions, and involvement in neurological disorders. Chemistry and physics of lipids. 2000;106(1):1-29. PubMed PMID: 10878232.

61. Zufferey R, Pirani K, Cheung-See-Kit M, Lee S, Williams TA, Chen DG, et al. The Trypanosoma brucei dihydroxyacetonephosphate acyltransferase TbDAT is dispensable for normal growth but important for synthesis of ether glycerophospholipids. PloS one. 2017;12(7):e0181432. doi: 10.1371/journal.pone.0181432. PubMed PMID: 28715456; PubMed Central PMCID: PMC5513551.

62. Bartke N, Hannun YA. Bioactive sphingolipids: metabolism and function. Journal of lipid research. 2009;50 Suppl:S91-6. doi: 10.1194/jlr.R800080-JLR200. PubMed PMID: 19017611; PubMed Central PMCID: PMC2674734.

63. Hannun YA, Obeid LM. Principles of bioactive lipid signalling: lessons from sphingolipids. Nature reviews Molecular cell biology. 2008;9(2):139-50. doi: 10.1038/nrm2329. PubMed PMID: 18216770.

64. Fukaya T, Gondaira T, Kashiyae Y, Kotani S, Ishikura Y, Fujikawa S, et al. Arachidonic acid preserves hippocampal neuron membrane fluidity in senescent rats. Neurobiology of aging. 2007;28(8):1179-86. doi: 10.1016/j.neurobiolaging.2006.05.023. PubMed PMID: 16790296.

65. Wang ZJ, Liang CL, Li GM, Yu CY, Yin M. Neuroprotective effects of arachidonic acid against oxidative stress on rat hippocampal slices. Chemico-biological interactions. 2006;163(3):207-17. doi: 10.1016/j.cbi.2006.08.005. PubMed PMID: 16982041.

66. Jing Y, Cui D, Bao F, Hu Z, Qin Z, Hu Y. Tryptophan deficiency affects organ growth by retarding cell expansion in Arabidopsis. The Plant journal : for cell and molecular biology. 2009;57(3):511-21. doi: 10.1111/j.1365-313X.2008.03706.x. PubMed PMID: 18980661.

67. Liu HN, Hu CA, Bai MM, Liu G, Tossou MCB, Xu K, et al. Short-term supplementation of isocaloric meals with L-tryptophan affects pig growth. Amino acids. 2017;49(12):2009-14. doi: 10.1007/s00726-017-2440-3. PubMed PMID: 28540509.

68. Liu Y, Yuan JM, Zhang LS, Zhang YR, Cai SM, Yu JH, et al. Effects of tryptophan supplementation on growth performance, antioxidative activity, and meat quality of ducks under high stocking density. Poultry science. 2015;94(8):1894-901. doi: 10.3382/ps/pev155. PubMed PMID: 26089478.

69. Shen YB, Voilque G, Kim JD, Odle J, Kim SW. Effects of increasing tryptophan intake on growth and physiological changes in nursery pigs. Journal of animal science. 2012;90(7):2264-75. doi: 10.2527/jas.2011-4203. PubMed PMID: 22287672.

70. Tsuji A, Nakata C, Sano M, Fukuwatari T, Shibata K. L-tryptophan metabolism in pregnant mice fed a high L-tryptophan diet and the effect on maternal, placental, and fetal growth. International journal of tryptophan research : IJTR. 2013;6:21-33. doi: 10.4137/IJTR.S12715. PubMed PMID: 24009424; PubMed Central PMCID: PMC3748091.

71. Zhang E, Dong S, Wang F, Tian X, Gao Q. Effects of l-tryptophan on the growth, intestinal enzyme activities and non-specific immune response of sea cucumber (Apostichopus japonicus Selenka) exposed to crowding stress. Fish & shellfish immunology. 2018;75:158-63. doi: 10.1016/j.fsi.2018.01.009. PubMed PMID: 29331348.

72. Aruoma OI, Spencer JP, Mahmood N. Protection against oxidative damage and cell death by the natural antioxidant ergothioneine. Food and chemical toxicology : an international journal published for the British Industrial Biological Research Association. 1999;37(11):1043-53. PubMed PMID: 10566875.

73. Cheah IK, Halliwell B. Ergothioneine; antioxidant potential, physiological function and role in

disease. Biochimica et biophysica acta. 2012;1822(5):784-93. doi: 10.1016/j.bbadis.2011.09.017. PubMed PMID: 22001064.

74. Cheah IK, Tang RM, Yew TS, Lim KH, Halliwell B. Administration of Pure Ergothioneine to Healthy Human Subjects: Uptake, Metabolism, and Effects on Biomarkers of Oxidative Damage and Inflammation. Antioxidants & redox signaling. 2017;26(5):193-206. doi: 10.1089/ars.2016.6778. PubMed PMID: 27488221.

75. Zhu BZ, Mao L, Fan RM, Zhu JG, Zhang YN, Wang J, et al. Ergothioneine prevents copper-induced oxidative damage to DNA and protein by forming a redox-inactive ergothioneine-copper complex. Chemical research in toxicology. 2011;24(1):30-4. doi: 10.1021/tx100214t. PubMed PMID: 21047085.

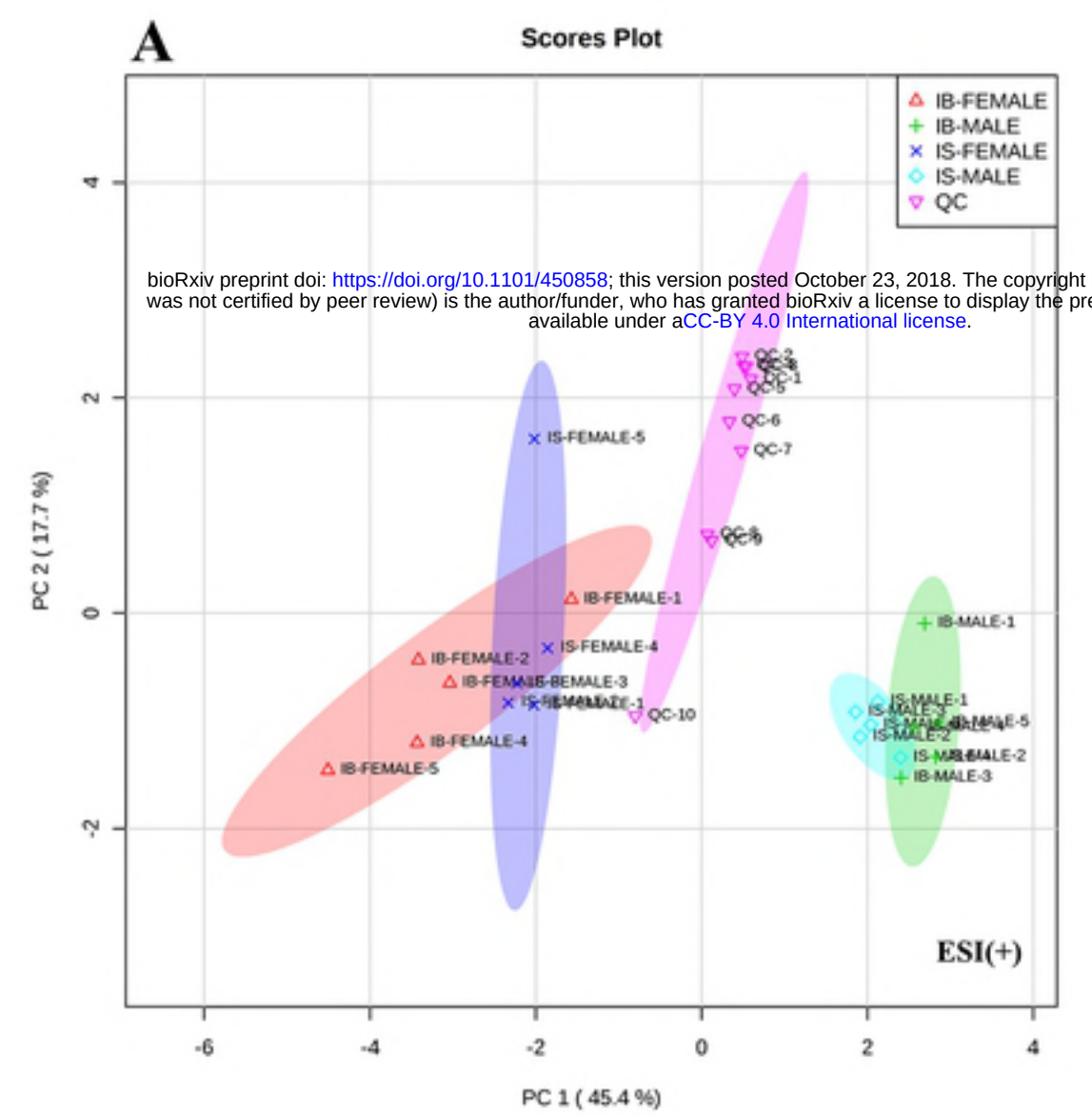

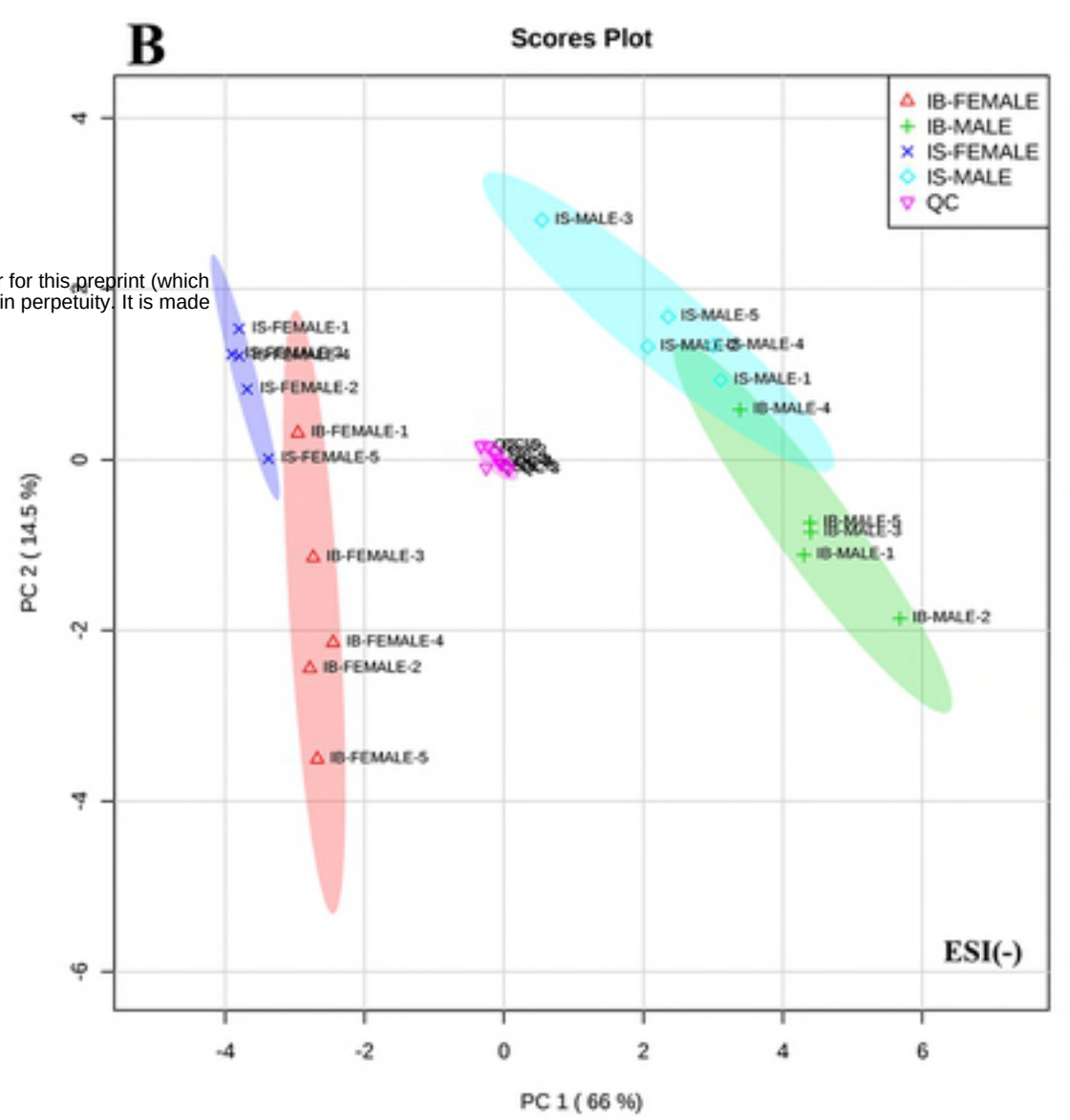

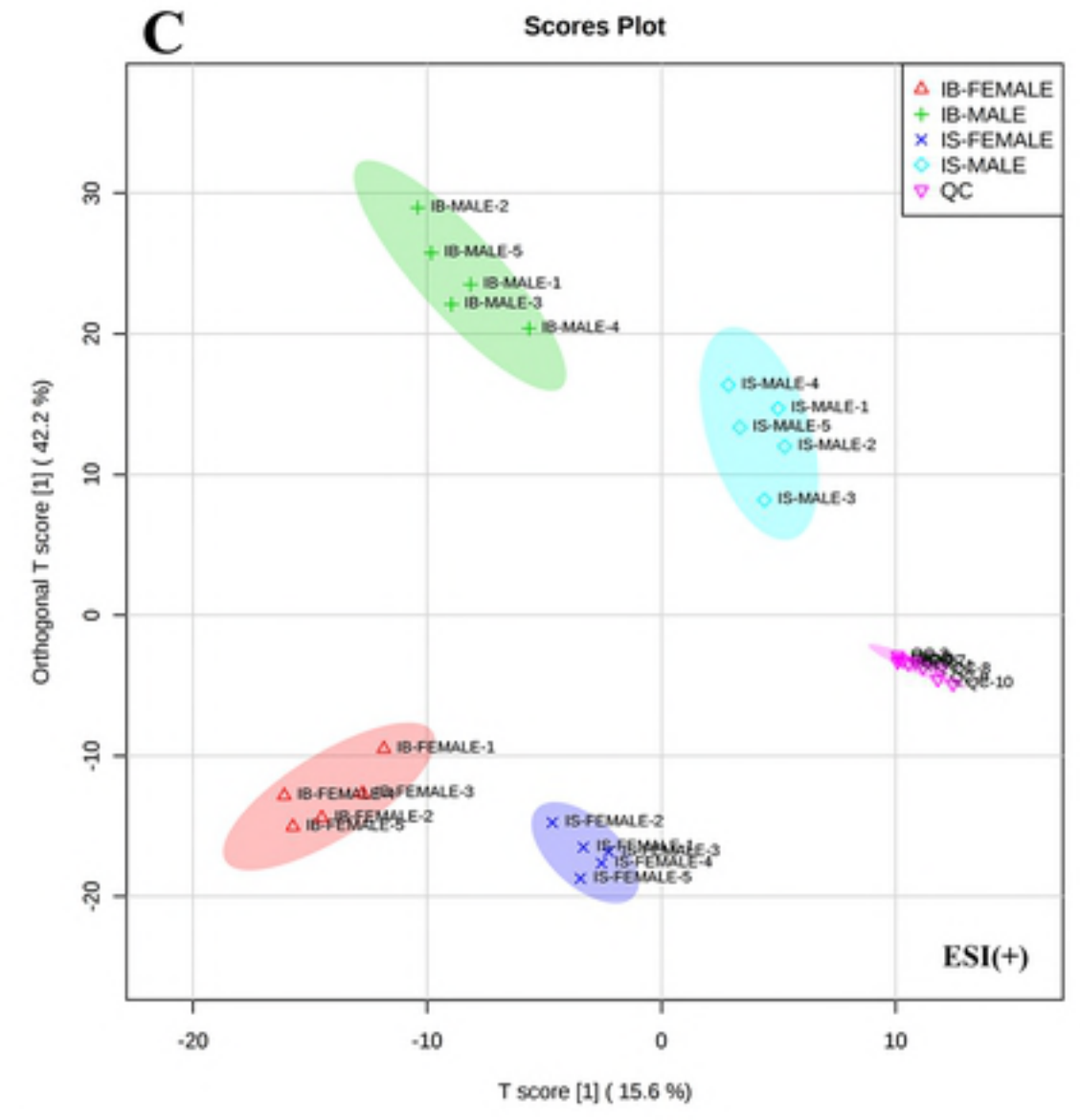

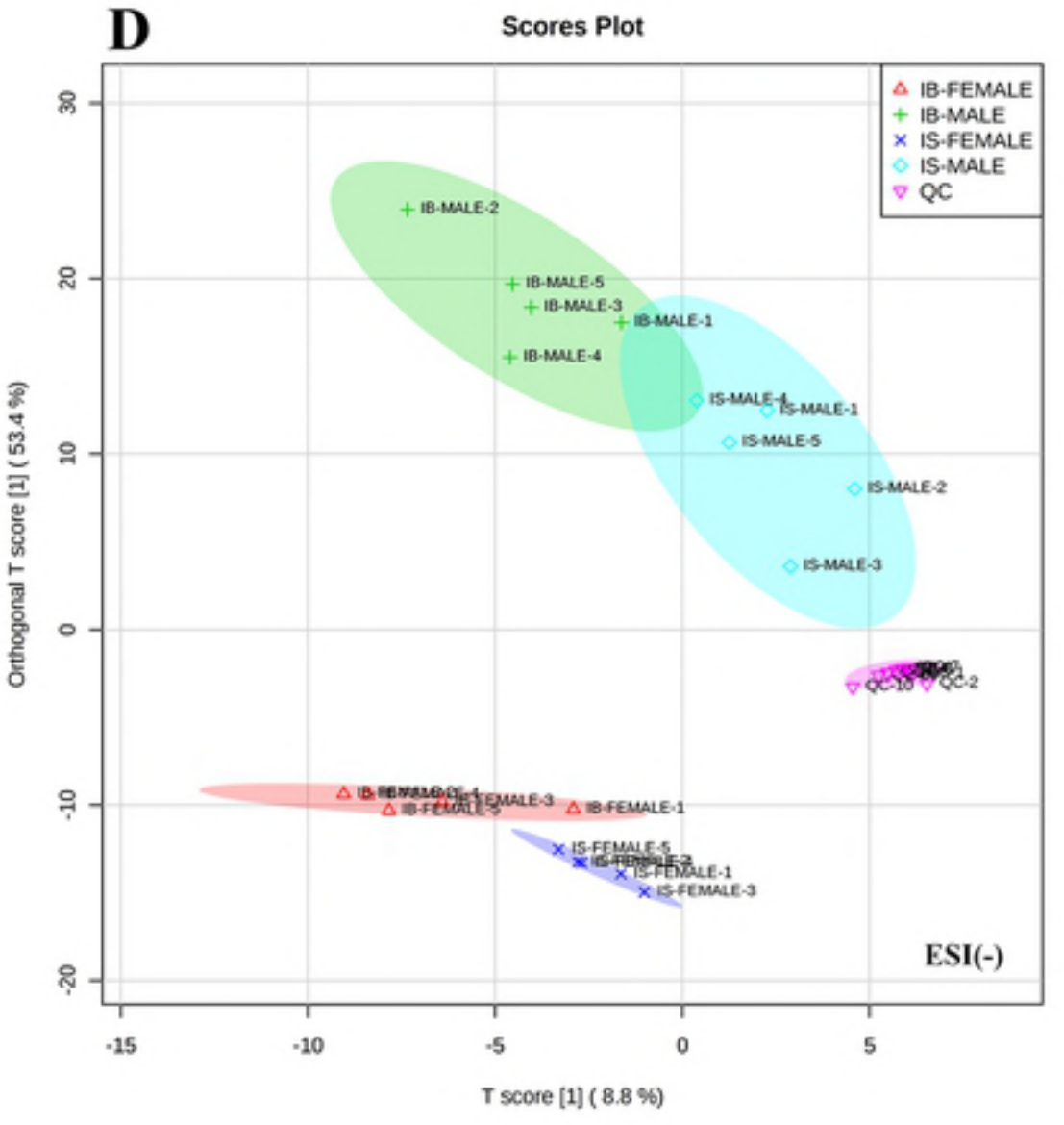

Figure 1

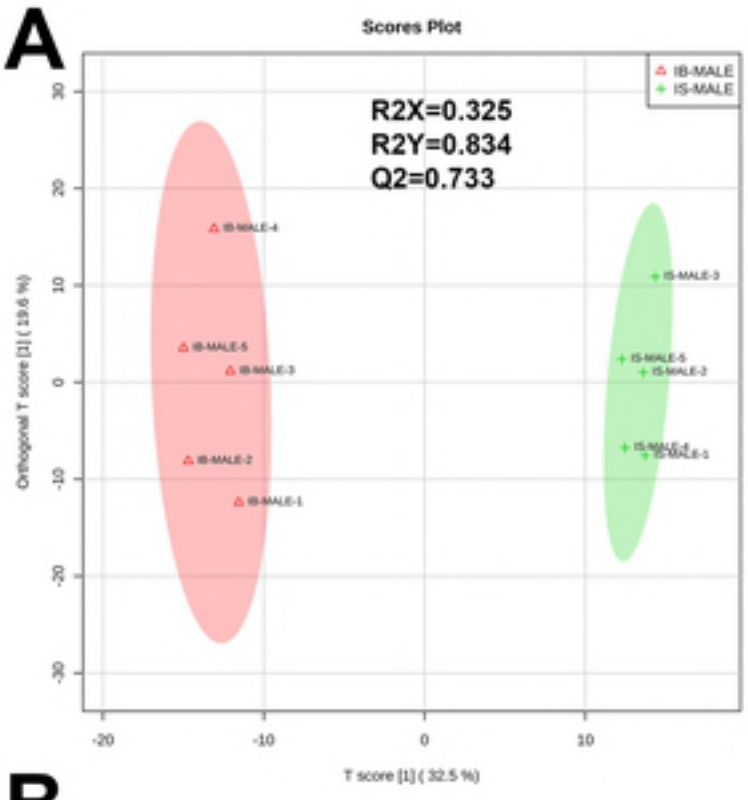

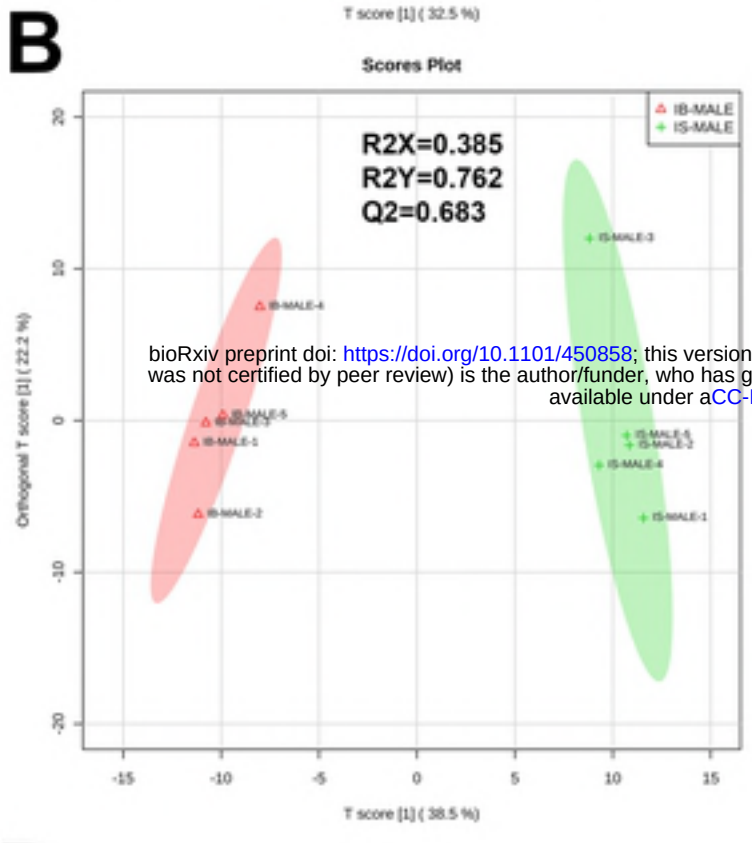

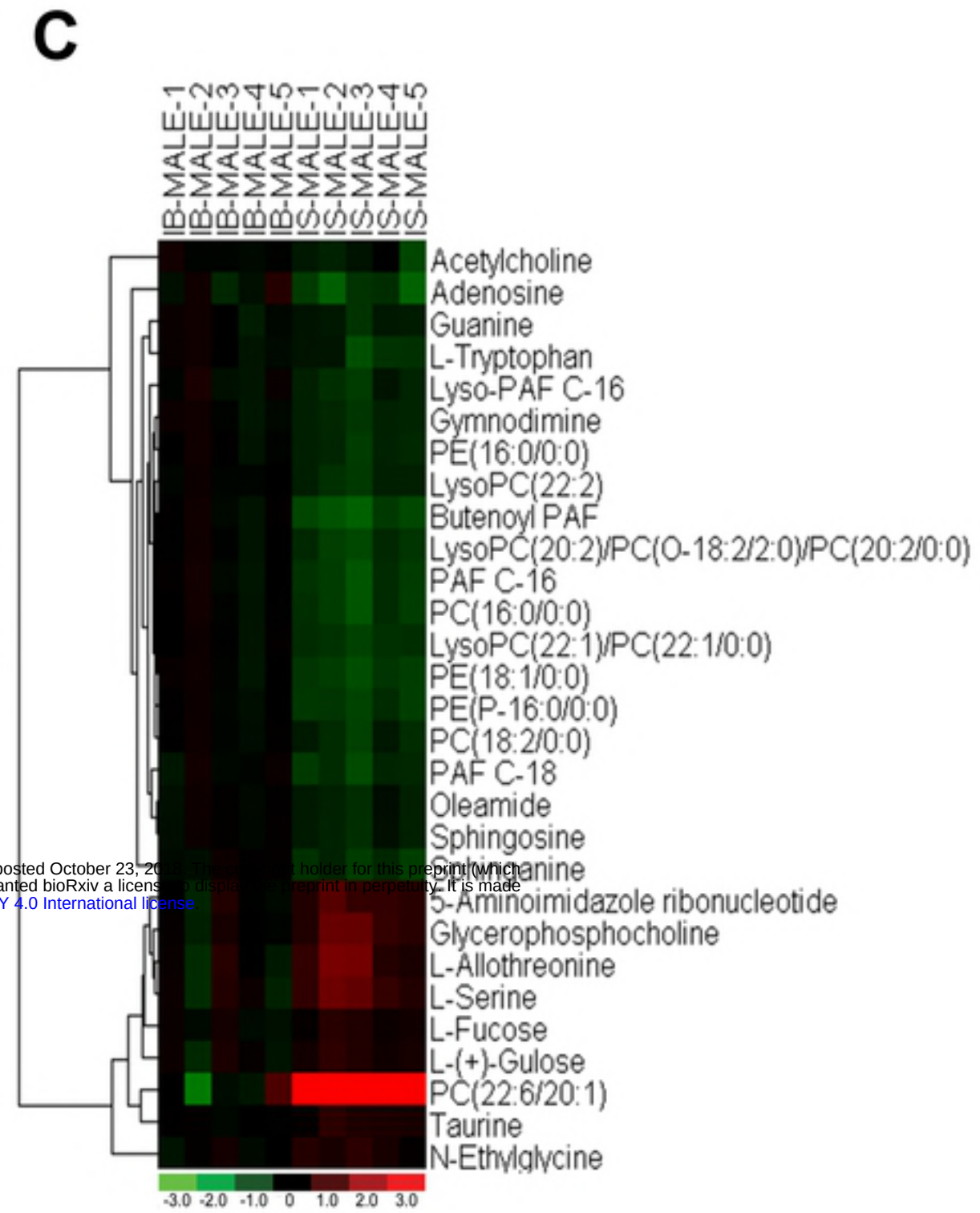

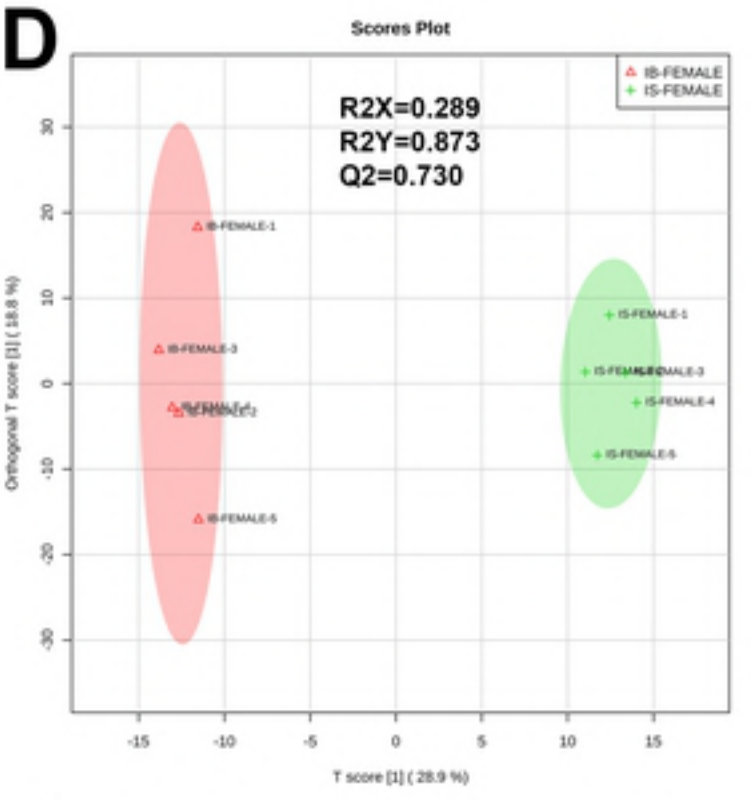

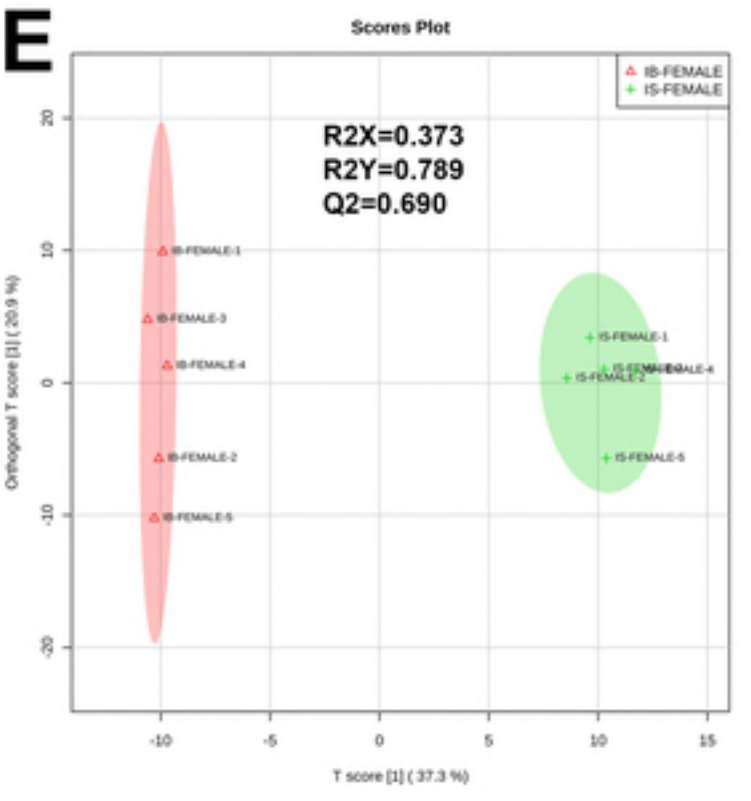

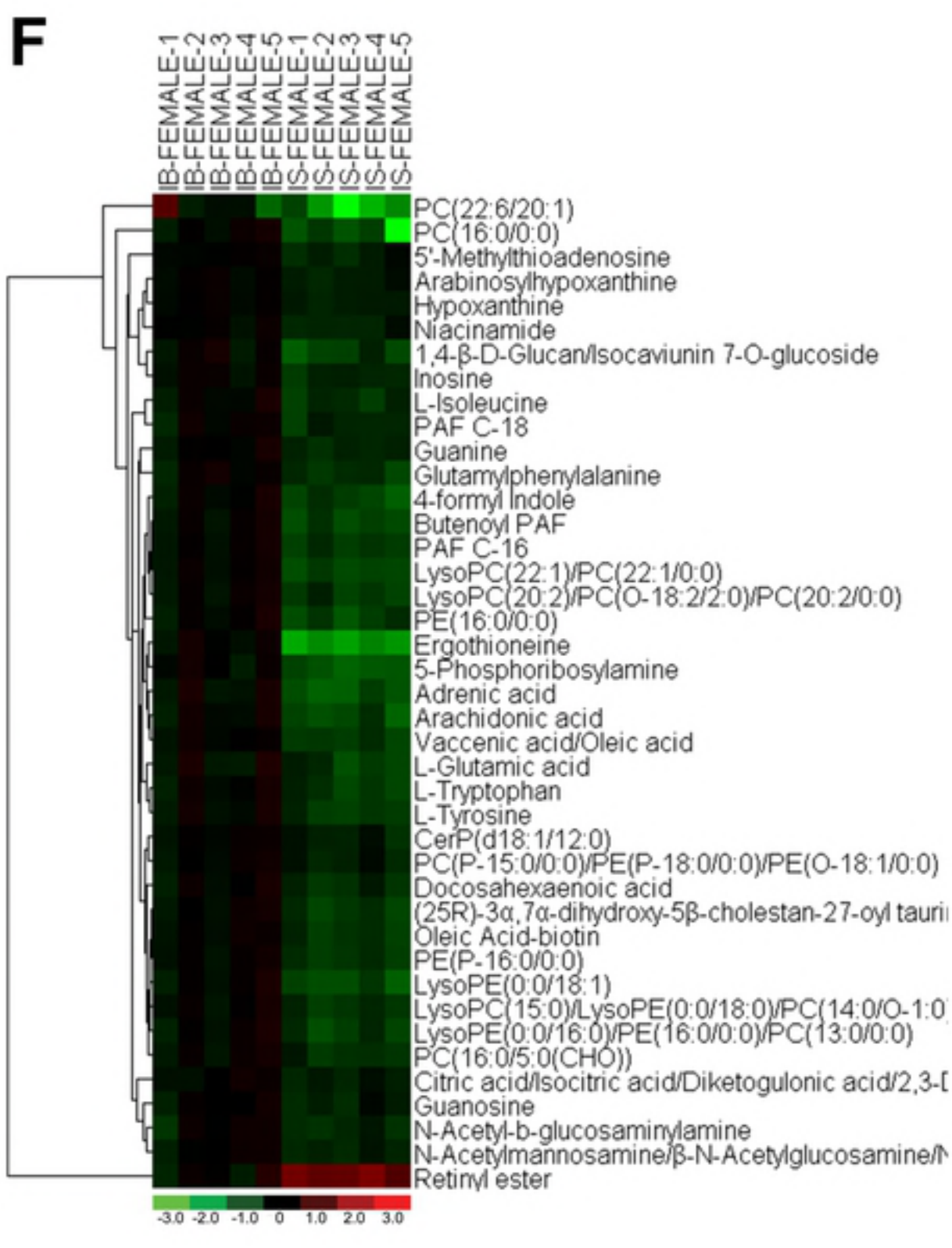

Figure 2

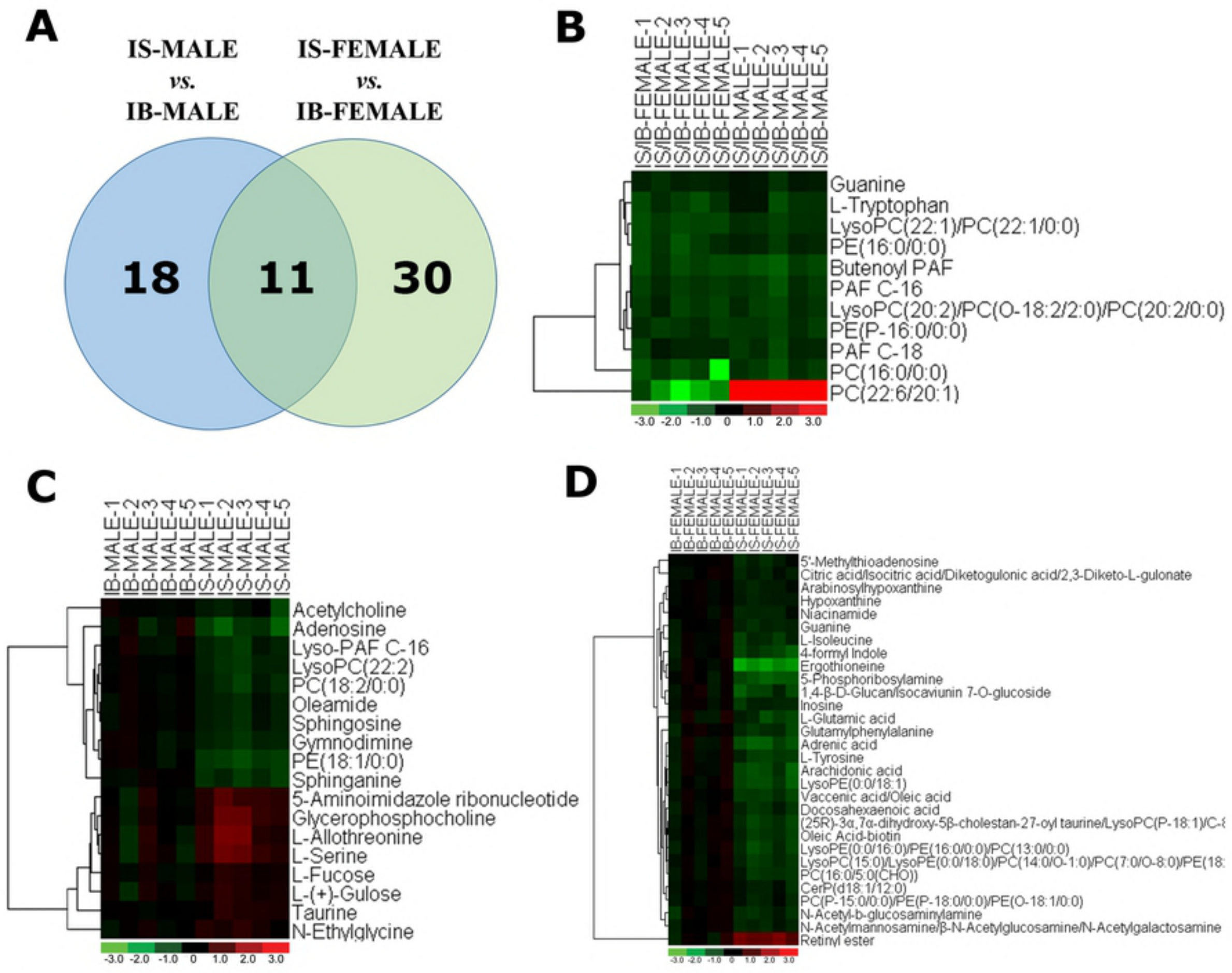
A
IS-MALE
vs.
IB-MALE
IS-FEMALE
vs.
IB-FEMALE
18
11
30
B
IS/IB-FEMALE-1
IS/IB-FEMALE-2
IS/IB-FEMALE-3
IS/IB-FEMALE-4
IS/IB-FEMALE-5
IS/IB-MALE-1
IS/IB-MALE-2
IS/IB-MALE-3
IS/IB-MALE-4
IS/IB-MALE-5
Guanine
L-Tryptophan
LysoPC(22:1)/PC(22:1/0:0)
PE(16:0/0:0)
Butenoyl PAF
PAF C-16
LysoPC(20:2)/PC(O-18:2/2:0)/PC(20:2/0:0)
PE(P-16:0/0:0)
PAF C-18
PC(16:0/0:0)
PC(22:6/20:1)
-3.0 -2.0 -1.0 0 1.0 2.0 3.0
C
IB-MALE-1
IB-MALE-2
IB-MALE-3
IB-MALE-4
IB-MALE-5
IS-MALE-1
IS-MALE-2
IS-MALE-3
IS-MALE-4
IS-MALE-5
Acetylcholine
Adenosine
Lyso-PAF C-16
LysoPC(22:2)
PC(18:2/0:0)
Oleamide
Sphingosine
Gymnodimine
PE(18:1/0:0)
Sphinganine
5-Aminoimidazole ribonucleotide
Glycerophosphocholine
L-Allothreonine
L-Serine
L-Fucose
L-(+)-Gulose
Taurine
N-Ethylglycine
-3.0 -2.0 -1.0 0 1.0 2.0 3.0
D
5'-Methylthioadenosine
Citric acid/Isocitric acid/Diketogulonic acid/2,3-Diketo-L-gulonate
Arabinosylhypoxanthine
Hypoxanthine
Niacinamide
Guanine
L-Isoleucine
4-formyl Indole
Ergothioneine
5-Phosphoribosylamine
1,4-β-D-Glucan/Isocaviunin 7-O-glucoside
Inosine
L-Glutamic acid
Glutamylphenylalanine
Adrenic acid
L-Tyrosine
Arachidonic acid
LysoPE(0:0/18:1)
Vaccenic acid/Oleic acid
Docosahexaenoic acid
Oleic Acid-biotin
LysoPE(0:0/16:0)/PE(16:0/0:0)/PC(13:0/0:0)
PC(16:0/5:0(CHO))
CerP(d18:1/12:0)
PC(P-15:0/0:0)/PE(P-18:0/0:0)/PE(O-18:1/0:0)
N-Acetyl-b-glucosaminylamine
Retinyl ester

Figure 3

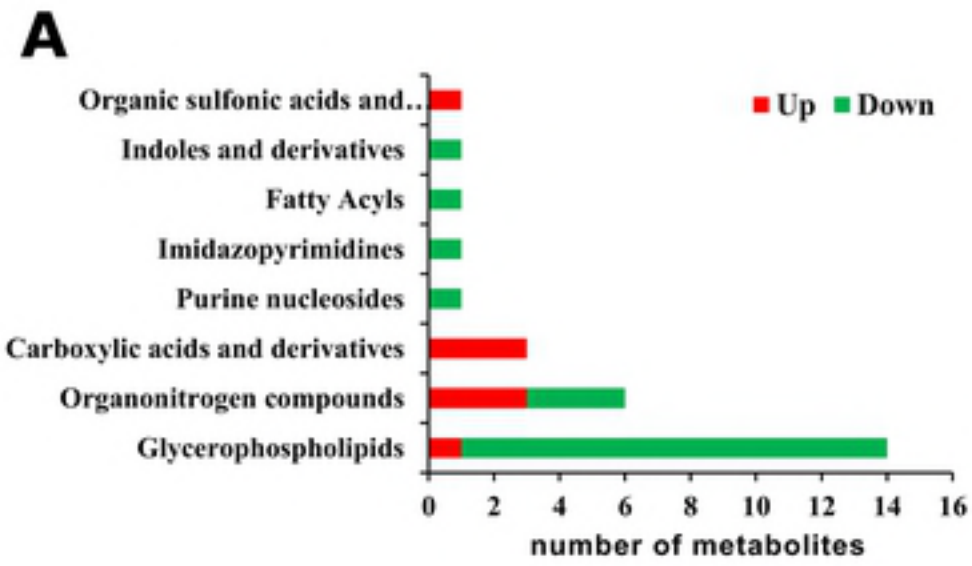

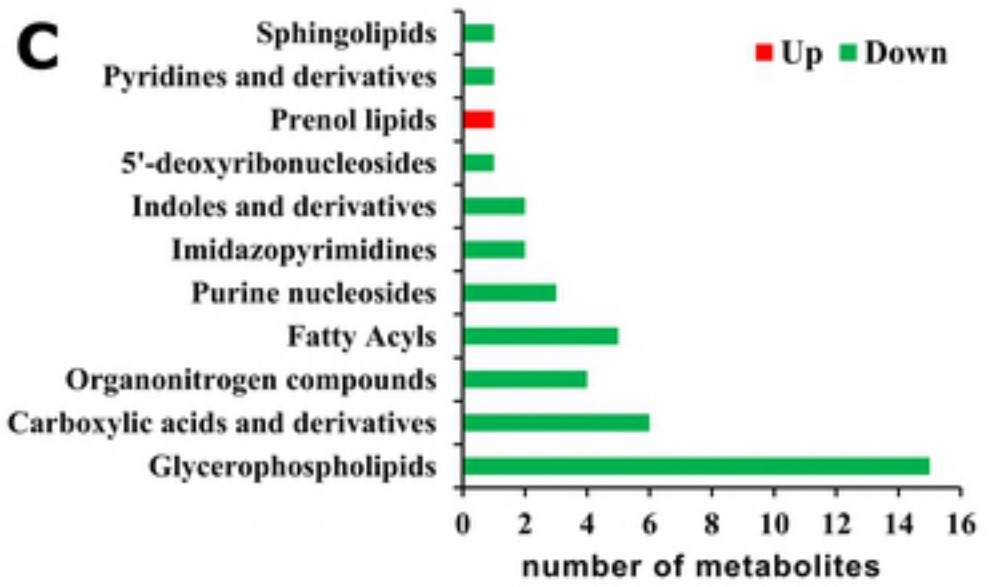

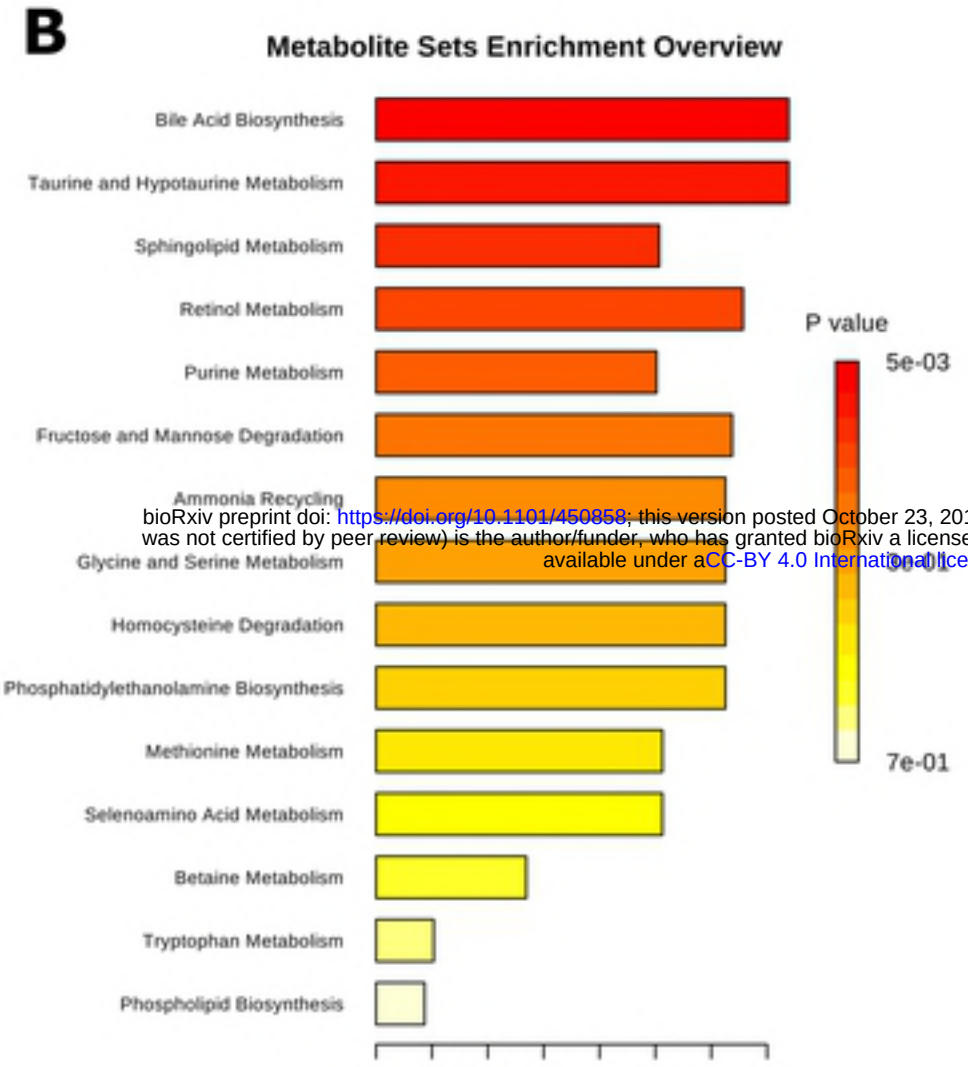

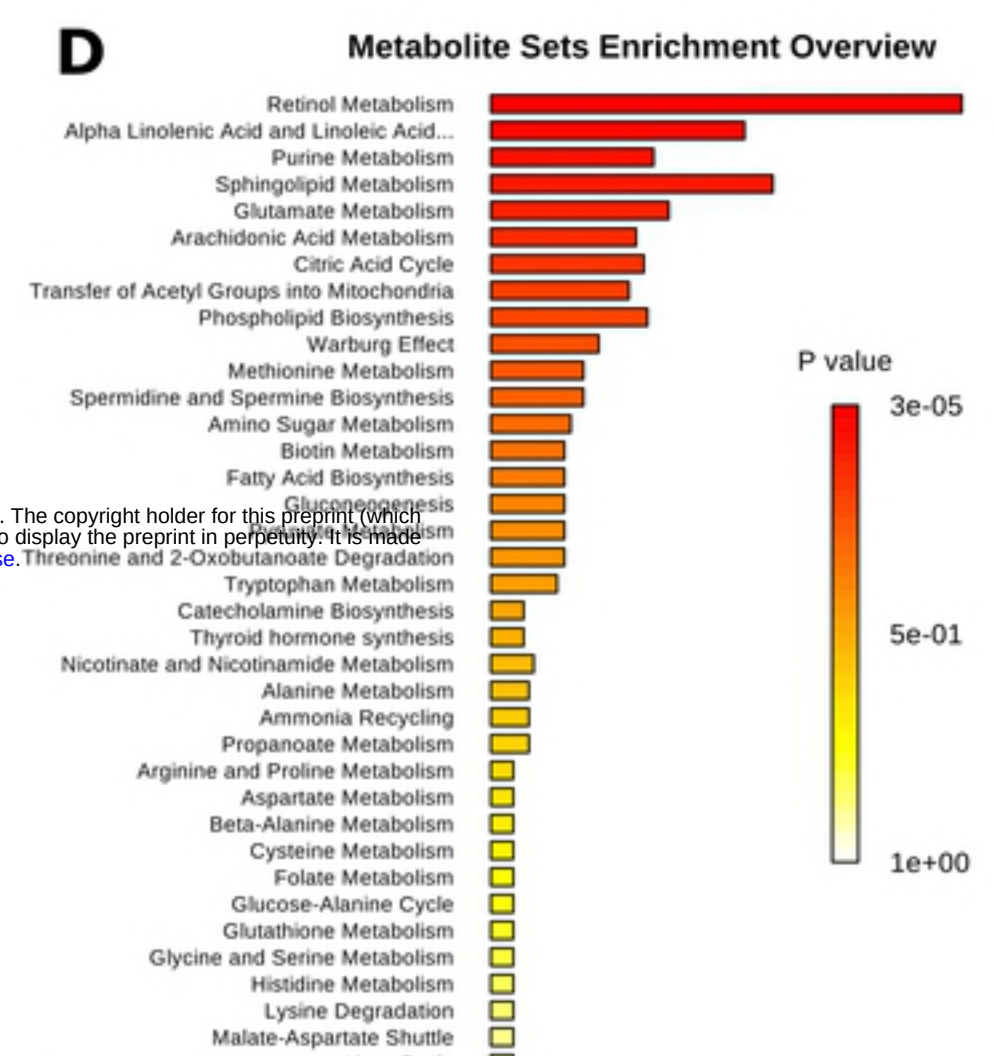

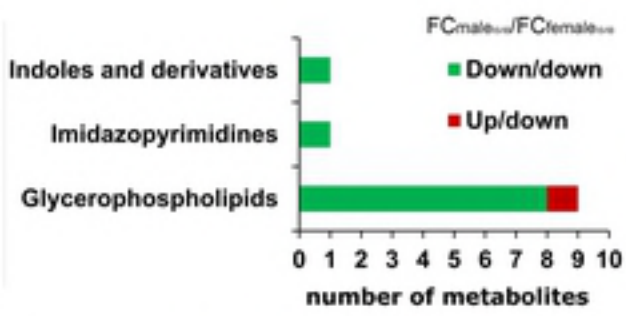

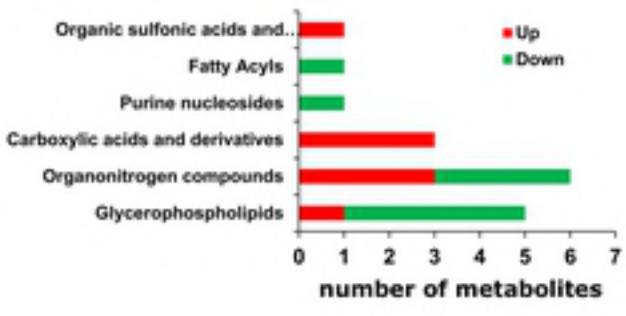

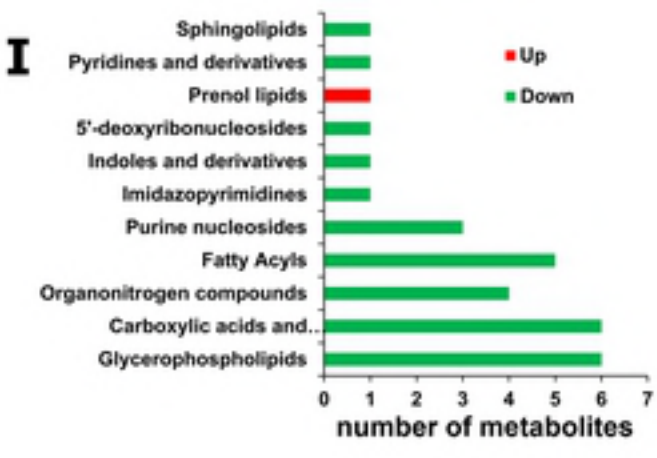

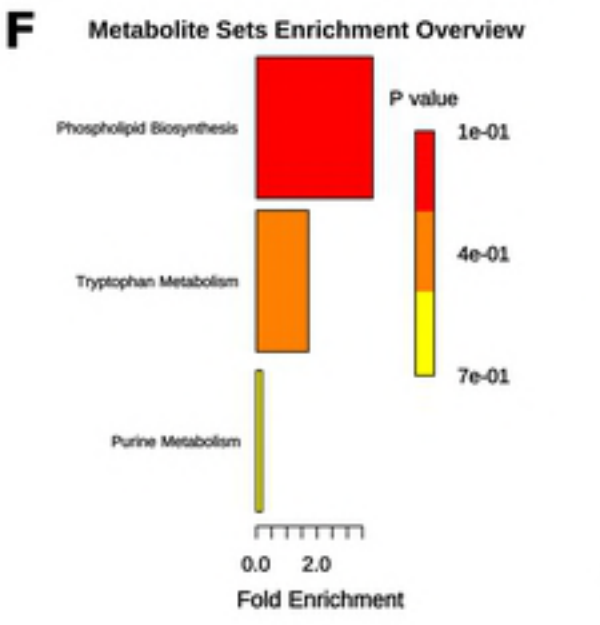

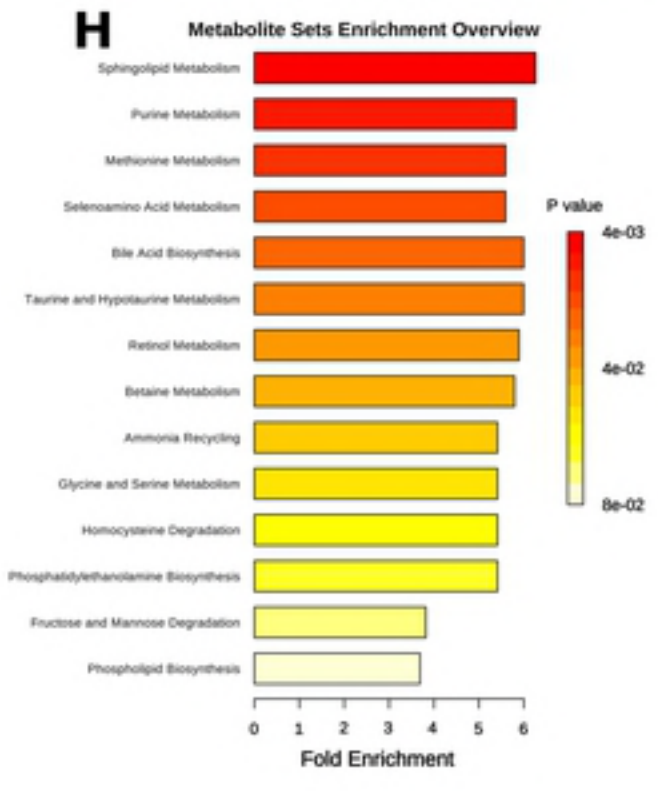

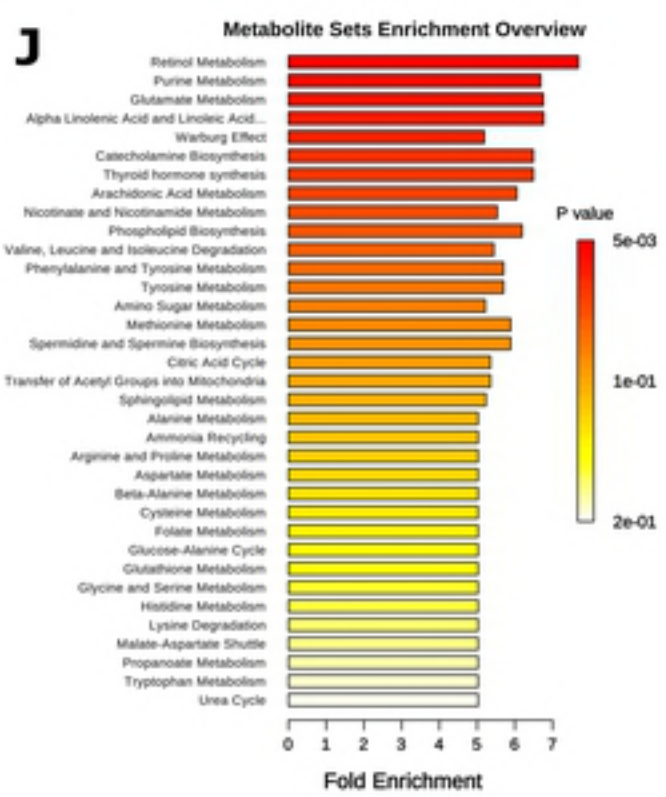

Figure 4

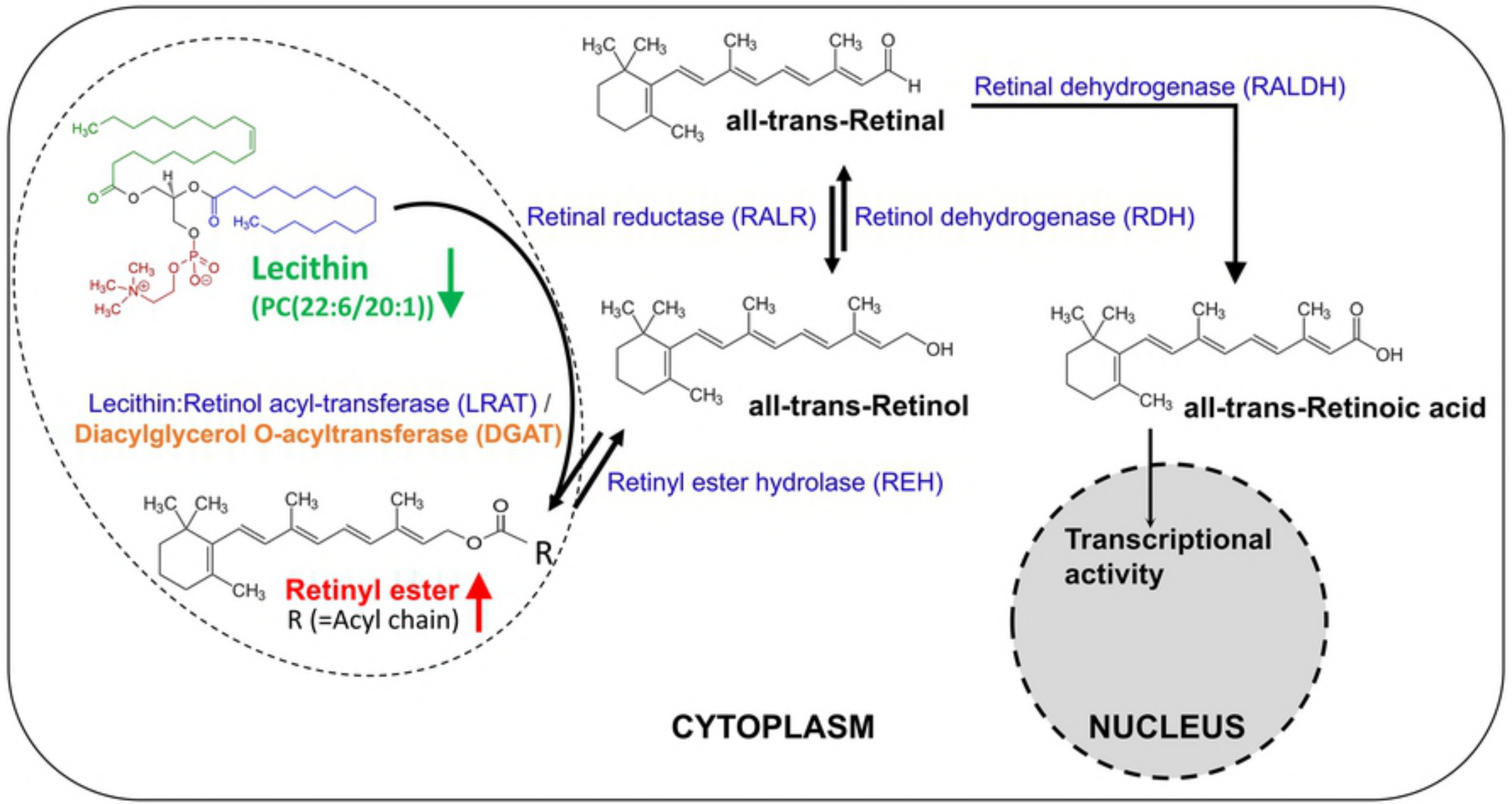
all-trans-Retinal
Retinal dehydrogenase (RALDH)
Retinal reductase (RALR)
Retinol dehydrogenase (RDH)
Lecithin
(PC(22:6/20:1))
all-trans-Retinol
all-trans-Retinoic acid
Lecithin:Retinol acyl-transferase (LRAT) /
Diacylglycerol O-acyltransferase (DGAT)
Retinyl ester hydrolase (REH)
Retinyl ester
R (=Acyl chain)
Transcriptional
activity
CYTOPLASM
NUCLEUS

Figure 5

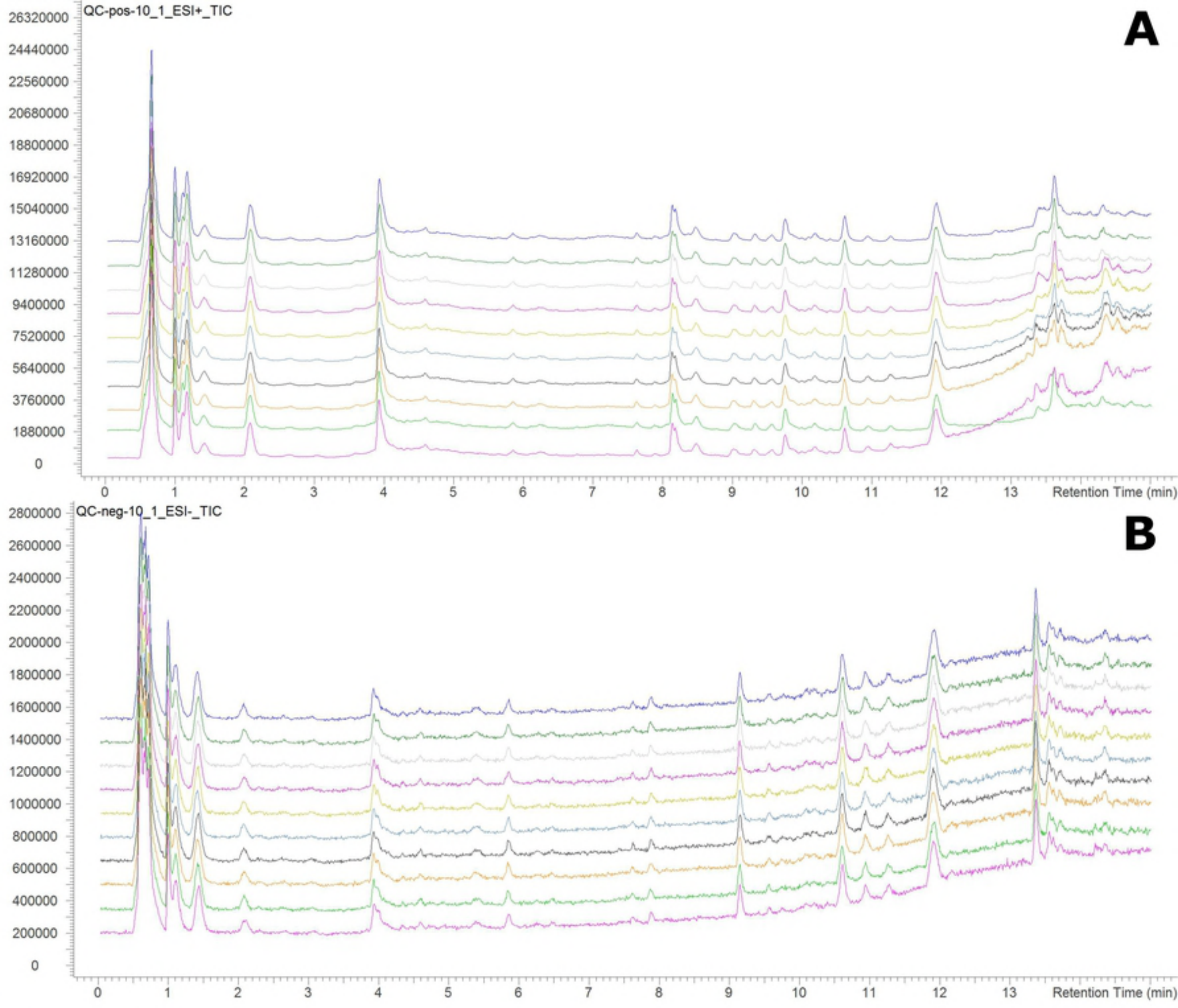
QC-pos-10_1_ESI+_TIC
A
26320000
24440000
22560000
20680000
18800000
16920000
15040000
13160000
11280000
9400000
7520000
5640000
3760000
1880000
0
0
1
2
3
4
5
6
7
8
9
10
11
12
13
Retention Time (min)
QC-neg-10_1_ESI-_TIC
B
2800000
2600000
2400000
2200000
2000000
1800000
1600000
1400000
1200000
1000000
800000
600000
400000
200000
0
0
1
2
3
4
5
6
7
8
9
10
11
12
13
Retention Time (min)

Figure S1

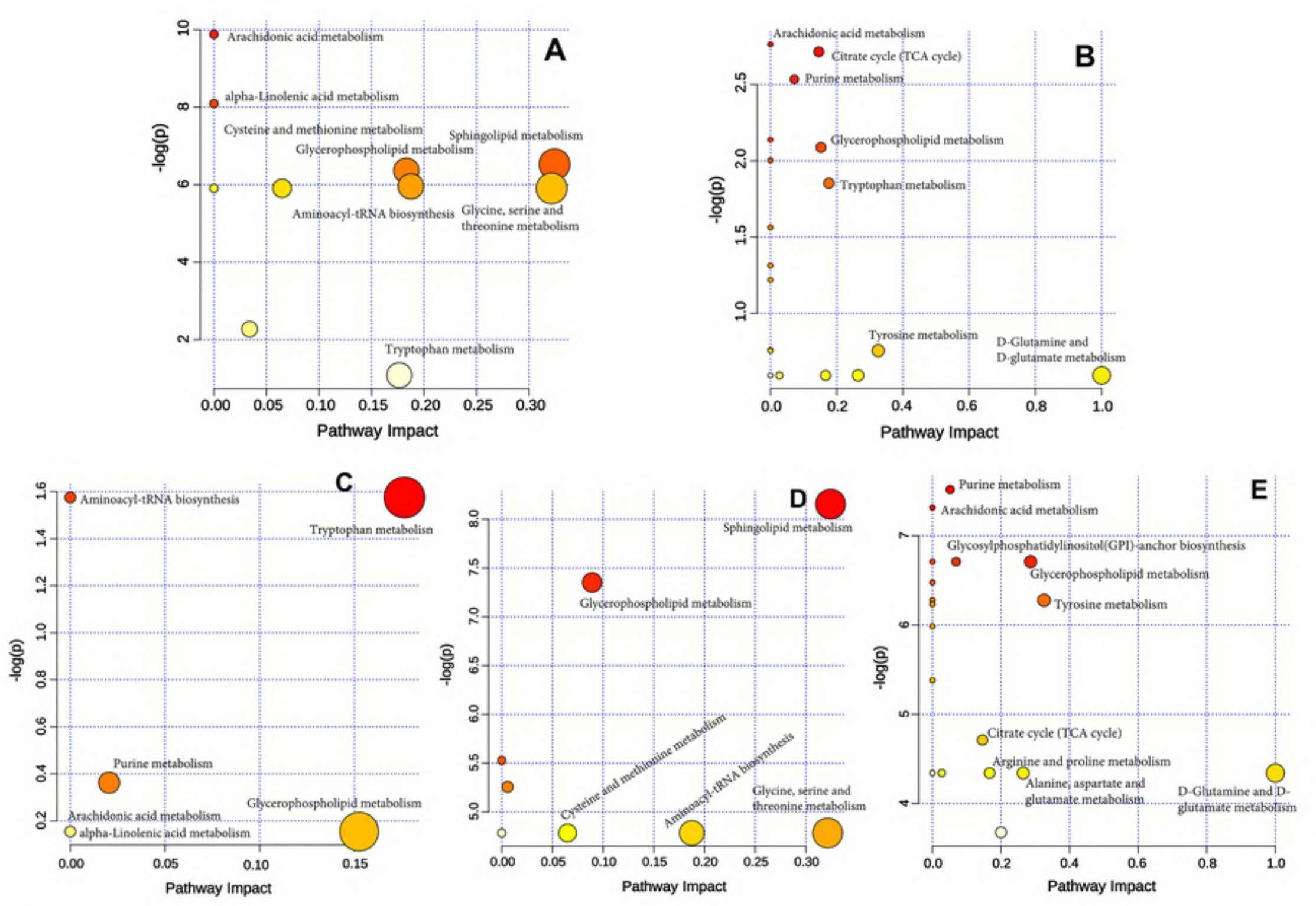
A
Arachidonic acid metabolism
alpha-Linolenic acid metabolism
Cysteine and methionine metabolism
Glycerophospholipid metabolism
Sphingolipid metabolism
Aminoacyl-tRNA biosynthesis
Glycine, serine and threonine metabolism
Tryptophan metabolism
-log(p)
Pathway Impact
B
Arachidonic acid metabolism
Citrate cycle (TCA cycle)
Purine metabolism
Glycerophospholipid metabolism
Tryptophan metabolism
Tyrosine metabolism
D-Glutamine and D-glutamate metabolism
-log(p)
Pathway Impact
C
Aminoacyl-tRNA biosynthesis
Tryptophan metabolism
Purine metabolism
Glycerophospholipid metabolism
Arachidonic acid metabolism
alpha-Linolenic acid metabolism
-log(p)
Pathway Impact
D
Sphingolipid metabolism
Glycerophospholipid metabolism
Cysteine and methionine metabolism
Aminoacyl-tRNA biosynthesis
Glycine, serine and threonine metabolism
-log(p)
Pathway Impact
E
Purine metabolism
Arachidonic acid metabolism
Glycosylphosphatidylinositol(GPI)-anchor biosynthesis
Glycerophospholipid metabolism
Tyrosine metabolism
Citrate cycle (TCA cycle)
Arginine and proline metabolism
Alanine, aspartate and glutamate metabolism
D-Glutamine and D-glutamate metabolism
-log(p)
Pathway Impact

Figure S2